Trade-off between solar photovoltaic panels and solar thermal collectors in collective (multi-)energy districts from an economic and ecological point of view

De Wolf Thomas

Academiejaar 2023 – 2024

Preface

This thesis represents my final academic work in completing the Master of Engineering in Energy at KU Leuven. I am grateful for the opportunity to work on my first-choice topic, focusing on renewable energies in residential districts. Engaging in this project contributed to my personal growth and deepened my understanding, complementing my academic journey. I want to thank my daily advisors, Louis, Naomi, and Anna, for sharing their enthusiasm and valuable insights on the topic. I am grateful for your guidance and patience during our numerous meetings, which enabled me to make steady progress and work more efficiently. Your support kept me motivated and helped me overcome the challenges I encountered. I would also like to thank my promoter, Prof. Helsen, for organizing this thesis topic and for the feedback sessions throughout the year. These sessions were a source of inspiration and boosted my confidence, allowing me to produce a higher quality of work. Finally, I want to thank the jury for their feedback during my intermediate thesis defense, as well as for their time in reading and evaluating this thesis.

De Wolf Thomas

Contents

Abstract

In the pursuit of climate goals and a carbon-neutral future, the building sector—known for its high energy consumption—has become a critical focus. Renewable energy solutions such as photovoltaic (PV) panels, solar thermal collectors (STCs) are particularly relevant, especially when integrated into community energy systems, often referred to as energy districts. These systems, which share components like heat pumps, energy storage, batteries, PV panels, and STCs, are designed to optimize energy generation, distribution, and utilization within a localized area, with a strong emphasis on sustainability and efficiency. However, the limited space available for centralized panel fields in these districts, coupled with the restricted roof area on individual dwellings, necessitates a trade-off between PV panels and STCs. This thesis examines four virtual low-carbon residential energy systems in Belgium that incorporate rooftop PV panels and STCs, providing heating, cooling, domestic hot water, and electricity. These systems also include a residential battery and a collective district heating network with seasonal borehole thermal energy storage to optimize the use of excess PV and STC energy. The energy flows within these systems are modeled to assess the performance of PV panels and STCs in terms of Total Cost of Ownership (TCO) and operational CO_2 emissions, evaluating the economic and ecological trade-offs between them. Additionally, a sensitivity analysis is conducted on influential parameters and cost data with high variability to establish robust guidelines for the use of solar PV and STCs. The results indicate that the trade-off between PV panels and STCs in collective residential energy systems is complex. While most cases tend to favor full PV, some cases reveal an optimal configuration that includes a few STCs, depending on the performance indicator (TCO or CO_2 emissions) and the specific boundary conditions in which they operate.

Samenvatting

Bij het nastreven van klimaatdoelstellingen en een CO_2-neutrale toekomst is de bouwsector - bekend om zijn hoge energieverbruik - een belangrijk aandachtspunt geworden. Hernieuwbare energieoplossingen zoals fotovoltaïsche (PV) panelen, thermische zonnecollectoren (STC's) zijn bijzonder relevant, vooral wanneer ze geïntegreerd zijn in gemeenschappelijke energiesystemen, vaak energiewijken genoemd. Deze systemen, met componenten zoals warmtepompen, energieopslag, batterijen, PV-panelen en STC's, zijn ontworpen om de opwekking, distributie en het gebruik van energie binnen een gelokaliseerd gebied te optimaliseren, met een sterke nadruk op duurzaamheid en efficiëntie. De beperkte ruimte die beschikbaar is voor centrale panelenvelden in deze wijken, in combinatie met het beperkte dakoppervlak van individuele woningen, maakt echter een afweging tussen PV-panelen en STC's noodzakelijk. Deze thesis onderzoekt vier virtuele CO_2-arme residentiële energiesystemen in België die PV-panelen en STC's op het dak bevatten, die verwarming, koeling, sanitair warm water en elektriciteit leveren. Deze systemen omvatten ook een residentiële batterij en een collectief stadsverwarmingsnetwerk met seizoensgebonden opslag van thermische energie in boorgaten om het gebruik van overtollige PV- en STC-energie te optimaliseren. De energiestromen binnen deze systemen worden gemodelleerd om de prestaties van PV-panelen en STC's te beoordelen in termen van Total Cost of Ownership (TCO) en operationele CO_2-uitstoot, waarbij de economische en ecologische afwegingen tussen beide worden geëvalueerd. Daarnaast wordt er een sensitiviteitsheidsanalyse uitgevoerd op invloedrijke parameters en kostengegevens met een hoge variabiliteit om robuuste richtlijnen op te stellen voor het gebruik van fotovoltaïsche panelen en STC's. De resultaten geven aan dat de afweging tussen PV-panelen en STC's in collectieve energiesystemen voor woningen complex is. Terwijl de meeste gevallen de voorkeur geven aan volledige PV, tonen sommige gevallen een optimale configuratie met een paar STC's, afhankelijk van de prestatie-indicator (TCO of CO_2 uitstoot) en de specifieke randvoorwaarden waarin ze werken.

List of Figures and Tables

List of Figures

List of Tables

List of Abbreviations and Symbols

Abbreviations

AC   Alternating Current
A-W   Air-Water
B   Booster
COP   Coefficient Of Performance
DC   Direct Current
DHW   Domestic Hot Water
HEX   Heat Exchanger
HP   Heat Pump
IC   Investment Cost
OC   Operational Cost
MC   Maintenance Cost
MPPT   Maximum Power Point Tracking
NOCT   Nominal Operating Cell Temperature
PV   Photovoltaic
STC   Solar Thermal Collector
TCO   Total Cost of Ownership

Symbols

A	Surface area
a	Heat pump COP curve coefficient
b	Heat pump COP curve coefficient
c	Speed of light
c_p	Specific heat capacity of 'x'
f	STC heat gain fraction for domestic hot water
G	Solar irradiance
h	District heating network loss factor
L	Length
n_{pv}	Number of PV panels
Q	Thermal energy
q	Specific thermal energy
R_b^*	Equivalent borehole resistance
r	Radius
r	Annual discount rate
T	Temperature
T_{amb}	Temperature of ambient air
T_{stc}^f	Temperature of STC working fluid
V	Volume
W	Electrical energy

Greek symbols:

η	Efficiency
γ	PV temperature coefficient
λ	Thermal conductivity
π	The number pi
ρ	Density

Chapter 1

Introduction

1.1 Problem Statement

All member states of the European Union have committed to reaching climate neutrality by 2050, as detailed in the European Green Deal [25]. This ambitious goal necessitates a shift from fossil fuels towards increased adoption of renewable energy sources across all energy-intensive sectors. Roughly 35% of European energy-related CO_2 emissions are emitted by the building sector. This makes the building sector a player in this transition. These emissions arise from direct energy use in space heating with fossil fuels, domestic hot water, and indirect emissions from electricity utilization for home appliances and cooling [26]. Consequently, there is a pressing need to replace the systems providing these energy demands with more sustainable and cost-effective alternatives, such as heat pumps and renewable energy sources. This text focuses on low-carbon solutions for residential space heating, domestic hot water, space cooling, and electricity generation.

Renewable solar energy, through technologies such as solar photovoltaic (PV) panels and solar thermal collectors (STC), presents a viable low-carbon alternative to fossil fuels. Solar PV panels generate electricity, while STC systems deliver heat. However, the intermittent nature of solar energy, with availability often mismatched to demand, necessitates the incorporation of energy storage solutions. Battery storage can capture excess PV electricity generated during the day for use in the evening and night. Additionally, since solar energy is predominantly available in summer while heating needs peak in winter, a residential district heating system integrated with seasonal thermal energy storage provides a solution. This approach stores solar thermal energy during the summer for use in the winter, leveraging collective infrastructure benefits. Despite these advantages, the initial investment and operational costs associated with renewable energy systems and storage units warrant a thorough economic evaluation.

In residential settings, limited roof space often restricts the deployment of large-scale solar installations. This constraint requires a balance between rooftop PV and STC systems. This text examines virtual low-carbon residential district systems, focusing on the trade-off between PV and STC from both economic and ecological perspectives. The analysis considers the cost-effectiveness and CO_2 emission reductions of these systems to determine the optimal configuration for sustainable residential energy solutions.

1.2 Research Questions

To properly investigate the trade-off between PV and STC in low-carbon residential applications, this text is organized around three research questions:

- *What are low-carbon systems for residential districts with PV panels and STCs for which a trade-off between these panels exists?*

- *What are the CO_2 emissions reductions and monetary savings associated with the trade-off between PV and STC?*

- *What factors influence the trade-off between PV and STC?*

1.3 Related Work

The trade-off between PV panels and STCs in the building sector has been investigated for single buildings from both ecological and economic perspectives. Generally, studies conclude that PV panels tend to perform better economically, while STCs are more advantageous from an ecological standpoint in current circumstances [27, 28]. A similar conclusion is drawn for a central PV or STC solar field delivering heat to consumers through a district heating network, where PV electricity is sold to the grid and used to generate heat for the district with a heat pump. It is important to acknowledge that the perceived performance of PV panels and STCs is highly influenced by factors such as solar irradiance, energy demand, the cost, and the carbon content of alternative energy supplies, such as grid electricity [27]. The trade-off may differ for distributed PV and STCs when implemented in a district heating system with seasonal thermal energy storage. This is because a fundamental advantage of distributed STCs is their ability to inject excess heat into the network to regenerate the collective thermal storage [29]. Determining the trade-off between distributed PV panels and STCs in these types of residential district heating systems is a gap in the literature that this text aims to address.

1.4 Thesis Outline

This thesis is divided in seven chapters:

Chapter 2 provides the theoretical foundation for the components used in the selected energy systems. It includes a literature review on these components and introduces key equations.

Chapter 3 outlines the procedure for selecting the systems, based on a combination of literature review and logical analysis. It then presents and explains the chosen systems, addressing the first research question.

Chapter 4 details the modeling approach used to assess the trade-off between PV and STC systems. It presents an overview of the energy flow calculation model, describes the input data, and introduces the performance indicators used in the analysis, specifically total cost of ownership and CO_2 emissions.

Chapter 5 is dedicated to modeling the system components. Each section covers a specific component, providing the relevant equations, sizing methodologies, and technical data.

Chapter 6 addresses the second and third research questions by analyzing the performance of various PV/STC configurations in the selected systems. It includes a sensitivity analysis to explore how different parameters affect the trade-off. Insights from this chapter are summarized in Section 6.5, which offers guidelines for the use of PV panels and STC.

Chapter 7 summarizes the key findings of the research and presents recommendations for future studies.

Chapter 2

Component Research

This thesis investigates the integration and performance of photovoltaic panels and solar thermal collectors within an energy system designed to provide electricity, heating, cooling, and domestic hot water. To facilitate a proper understanding of these systems, this chapter introduces the relevant system components through a comprehensive literature review. Each section elaborates on one component.

2.1 Photovoltaic Panel

A PV panel is a renewable source of electricity that absorbs solar irradiation and converts it into Direct Current (DC) electricity. The panel consists of interconnected solar cells, made from silicon semiconductor material. A PV panel or module is created by connecting multiple solar cells in series or parallel configurations to meet specific voltage and current requirements for practical applications. PV panels are often connected to a Maximum Power Point Tracking (MPPT) device, which adjusts the current and voltage to ensure optimal operation [30]. To increase power output, multiple PV panels are connected in parallel. The output power of a photovoltaic array consisting of n_{pv} panels is given by [31]:

$$P_{pv} = n_{pv} \cdot \eta_{pv} \cdot A_{pv} \cdot G \tag{2.1}$$

With η_{pv} representing the PV panel efficiency, A_{pv} [m^2] the surface of the panel, and G [W/m^2] the solar irradiance on one panel. The PV efficiency can be expressed as followes [31]:

$$\eta_{pv} = \eta_{pv,rated}(1 - \gamma(T_{cell} - NOCT)) \tag{2.2}$$

Where $\eta_{pv,rated}$ is the rated efficiency provided by the manufacturer. This rated power is defined for the panel when the PV cells are at the Nominal Operating Cell Temperature, $NOCT$. The PV efficiency drops as the PV cell temperature, T_{cell} [°C], rises. To account for this temperature dependency, a factor with a negative temperature coefficient, γ [°C^{-1}], is included to adjust the overall PV efficiency accordingly.

2.2 Home Battery

Home batteries are rechargeable electrical storage systems designed to store DC electricity by converting it into chemical energy. This stored energy can later be converted back into DC electricity when needed. To facilitate this process, batteries require a dedicated charger for both charging and discharging operations. In residential settings with intermittent PV installations, batteries are used to manage short-term energy fluctuations from the PV-generated electricity. PV panels generate electricity only when exposed to solar irradiation during the daytime, which often does not align with electricity demand [30]. In such scenarios, batteries enhance the self-utilization of PV electricity, thereby reducing dependence on external sources such as the electric grid [32].

2.3 Grid Connection

Most residential buildings are connected to the electrical power grid, which supports bidirectional energy flow for both consumption and feeding electricity back into the grid. These energy flows are typically managed on a kilowatt-hour (kWh) basis, with a price applied per kWh passing through the meter [30]. When residential properties are equipped with renewable electricity sources, such as PV installations, they can sell the electricity they generate at a feed-in tariff. This feed-in tariff is usually lower than the offtake tariff, which is the price at which electricity is purchased [32].

2.4 Hybrid Inverter

A hybrid inverter for residential applications acts as a central connection point between the PV panels, the home battery, domestic electricity demand, and the electricity grid, as illustrated in Figure 2.1. This device converts DC electricity into Alternating Current (AC) electricity, while also adjusting the voltage to match the requirements of various connections. AC connections are used for the grid and domestic loads, whereas DC connections are reserved for the PV panels and the battery. Note that both the connection to the grid and the connection to the battery are bidirectional. The primary objective of the hybrid inverter is to meet domestic electricity demand while optimizing the use of the PV panels, the battery, and the grid connection [1].

The hybrid inverter incorporates two key functionalities for the PV and battery connections. It features a maximum power point tracking device, which ensures that the PV panels operate at their optimal power generation levels. Additionally, the inverter includes battery charging and discharging functionality, enabling it to manage the battery's energy flow [33].
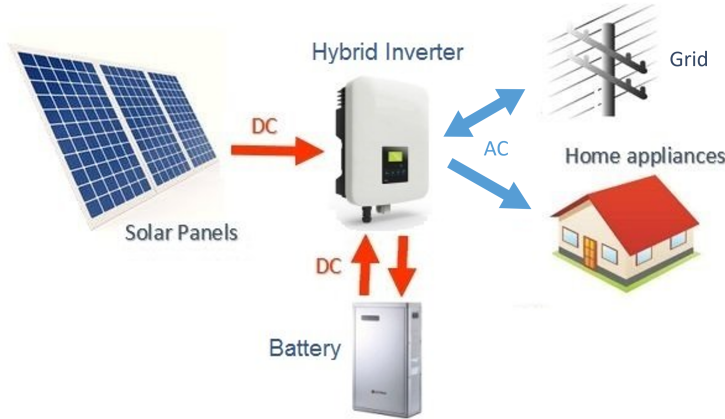
FIGURE 2.1: Layout of residential grid-connected PV-battery system (adapted from [1])

2.5 Flat Plate Solar Thermal Collector

Solar thermal collectors are a renewable source of heat. Active STCs capture solar energy and transfer it to a fluid medium, which then transfers the heat either to a storage unit or for direct use. Among the various types of STCs, the flat plate collector is commonly used in residential applications. The flat plate collector uses a water-glycol mixture as the working fluid that circulates through copper tubes. These tubes are surrounded by an absorber layer designed to maximize the absorption of incoming shortwave solar radiation, thereby raising the temperature of the fluid. The absorber layer should have a high thermal conductivity to efficiently transfer heat to the copper tubes. To increase the efficiency of the collector, several measures are taken to minimize heat losses. The collector is insulated on the shaded side to reduce thermal losses. In addition, the absorber has a low emissivity for long-wave infrared rays to reduce heat loss by radiation. Finally, a glass cover with a selective infrared blocking coating is added to the collector to further reduce heat emissions. [2, 34]. A schematic overview of the flat plate collector is presented in Figure 2.2.

2.5.1 Solar Thermal Collector Efficiency

The efficiency of the STC denotes [2]:

$$\eta_{\text{stc}} = \frac{\dot{Q}_{\text{stc}}}{G \cdot A_{\text{a}}} \tag{2.3}$$

Where $\dot{Q}_{stc}$ [W] is the heat output of the solar thermal collector, G is the solar radiation in W/m^2, and A_a [m^2] is the STC aperture area. The aperture area of a solar thermal collector is the area through which sunlight passes before it is absorbed. This area is smaller than the actual physical area of the collector and larger than the area of the collector absorber. All three areas are specified by the manufacturer.
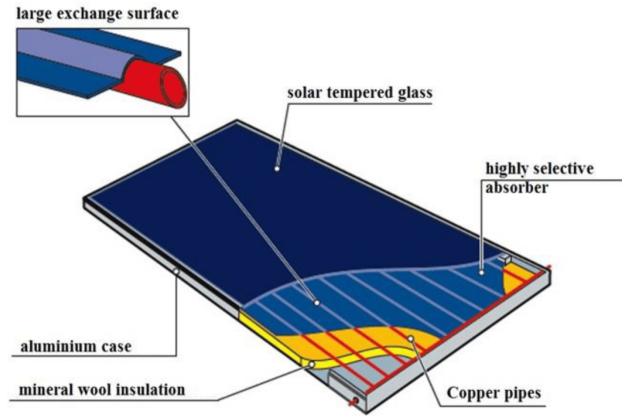
FIGURE 2.2: Schematic representation of the flat plate collector [2]

The STC efficiency η_{stc} is denoted by [34]:

$$\eta_{stc} = \eta_0 - k_1 \frac{T^f_{stc} - T_{amb}}{G} - k_2 \frac{(T^f_{stc} - T_{amb})^2}{G} \tag{2.4}$$

where η_0 is the optical efficiency, k_1 and k_2 are the effective heat loss coefficients respectively in $\mathrm{W/(m^2 \cdot K)}$ and $\mathrm{W/(m^2 \cdot K^2)}$. These three parameters characterize the performance of a solar thermal collector and are detailed in the collector's data sheet. The optical efficiency represents the theoretical maximum efficiency of the collector but is reduced by two correction terms. These correction terms depend on the solar irradiation and the temperature difference between the average STC fluid temperature, T^f_{stc} [°C], and the ambient air temperature, T_{amb} [°C]. As the temperature differential increases, the efficiency of the system decreases due to an increase in heat losses. Therefore collectors operate more efficiently at a lower working fluid temperature. The efficiency function can be fitted for the flat plate collector by entering the values of η_0, k_1, and k_2.

2.6 Heat Pump

A heat pump transfers heat from a low-temperature heat source to a high-temperature heat sink, utilizing electric energy. The electricity, denoted as $\dot{W}$, drives a thermo-dynamic compression-expansion cycle of a refrigerant fluid, as depicted in Figure 2.3. In this cycle, the refrigerant is first evaporated by absorbing heat $\dot{Q}_L$ from the low-temperature heat source at temperature T_L. The refrigerant is then compressed, increasing its pressure and temperature. It subsequently rejects heat $\dot{Q}_H$ to the high-temperature heat sink at temperature T_H, where it condenses. Finally, the refrigerant undergoes expansion through an expansion valve, reducing its pressure and temperature, and the cycle repeats [3].
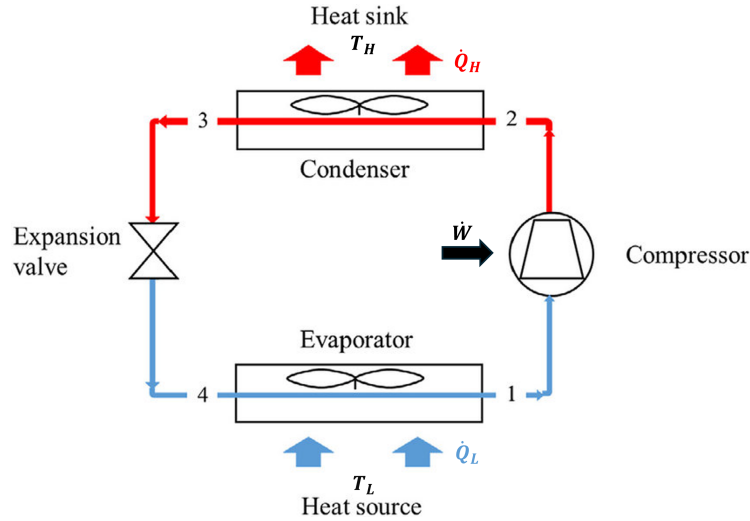
FIGURE 2.3: Schematic representation of the heat pump cycle (adapted from [3])

This thesis primarily focuses on the utilization of heat pumps as a residential heating solution. The low-temperature heat sources employed in this thesis include the surrounding air, soil, and a water supply, such as a district heating network (see section 2.9). In all cases, the heat extracted from these sources is rejected to a water supply. This heated water is then utilized for domestic hot water or space heating. Another domestic application of the heat pump is active space cooling. In the present case, dwellings are employed as a low-temperature heat source. The dwellings are cooled by extracting heat from them and rejecting it at a high-temperature heat sink. In fact, a single heat pump can be used for both heating and cooling. By reversing the flow of the refrigerant, the low-temperature evaporator becomes the high-temperature condenser and vice versa. Since the compressor is unidirectional, additional valves are required to redirect the refrigerant to the compressor.

A Coefficient Of Performance (COP) is a measure of a heat pump's performance in heating mode. In the case of a heat pump delivering heat $\dot{Q}_H$ [W] using electricity $\dot{W}$ [W], the COP is defined as:

$$COP = \frac{\dot{Q}_H}{\dot{W}} \tag{2.5}$$

In refrigeration mode, the Refrigeration Coefficient Of Performance (COP_R) is used. By cooling $\dot{Q}_L$ [W], the COP_R of the heat pump is defined as:

$$COP_R = \frac{\dot{Q}_L}{\dot{W}} \tag{2.6}$$

It is important to note that both performance coefficients are typically greater than one. This indicates that the useful heating or cooling power output is greater than the electricity input required to power the cycle. This characteristic enhances the appeal

of heat pumps, as they require less electricity compared to direct electrical heating, such as with electric resistance heaters. The laws of thermodynamics establish a theoretical maximum for both performance coefficients, known as the Carnot COP:

$$COP_{\text{carnot}} = \frac{T_H}{T_H - T_L} \qquad COP_{R, \text{ carnot}} = \frac{T_L}{T_H - T_L} \qquad (2.7)$$

With T_H and T_L both expressed in Kelvin. These formulas reveal that a smaller temperature difference between the heat source and sink leads to a higher COP, thereby enhancing the heat pump's performance.

2.7 Thermal Energy Storage

Thermal energy storage technologies are used to store thermal energy for later use, typically to balance heating or cooling supply and demand. Thermal energy storage units can be classified into two categories: short-term and seasonal. Seasonal thermal energy storage involves storing energy over extended periods, often spanning several months. It captures excess heat or cold during one season for utilization in another, thereby addressing seasonal variations in energy supply and demand. Short-term thermal energy storage, in contrast, is utilized to store energy for a duration of a few hours to a few days. This technology buffers thermal load irregularities reducing peak demand or avoiding the cycling of heat generation units.

2.7.1 Seasonal Borehole Thermal Energy Storage

Seasonal borehole thermal energy storage involves using the ground as a medium to store and retrieve thermal energy over extended periods. The system employs the use of boreholes drilled into the ground, wherein heat U-tube exchangers are installed to transfer heat to and from the surrounding ground. Heat is injected or extracted by circulating hot or cold water through the U-tubes [4]. Figure 2.4 illustrates such a heat exchanger setup and a complete array of these exchangers, known as a borefield. The heat exchangers are usually of uniform length and are spaced several meters apart, allowing the ground between them to serve as storage capacity.

During summer, excess heat from buildings or solar collectors is stored in the ground, raising the temperature of the surrounding soil. This stored heat can be extracted in winter using a ground-source heat pump to provide heating. As heat is extracted, the ground within the borefield cools down, and this cold can be stored for use in summer cooling. During the storage period, conductive heat losses occur to the surrounding ground.

The size of the borefield is expressed as the total borehole heat exchanger length of the boreholes combined. A larger borefield encompasses more ground around the heat exchangers, thereby increasing its storage capacity. Additionally, a larger borefield encompasses a greater heat exchanger surface area, enhancing its ability to handle larger charge and discharge power peaks. Since borehole thermal energy storage
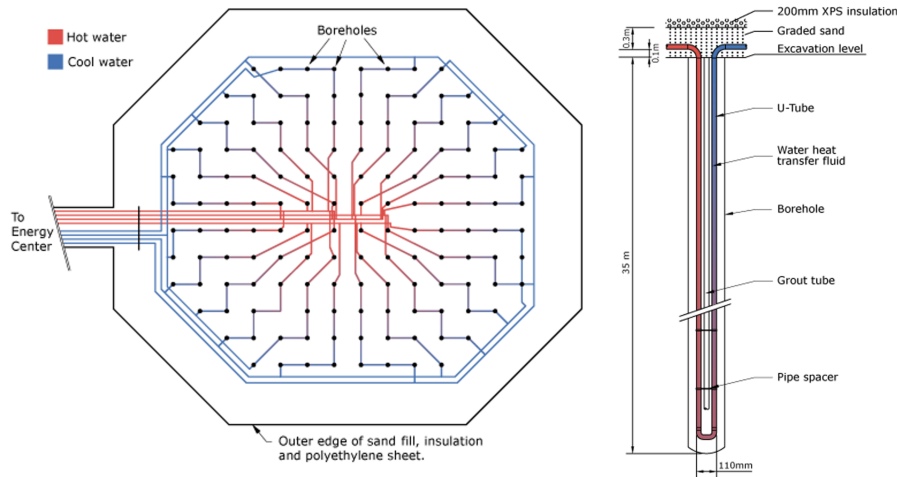
FIGURE 2.4: Borefield layout and single U-tube [4]
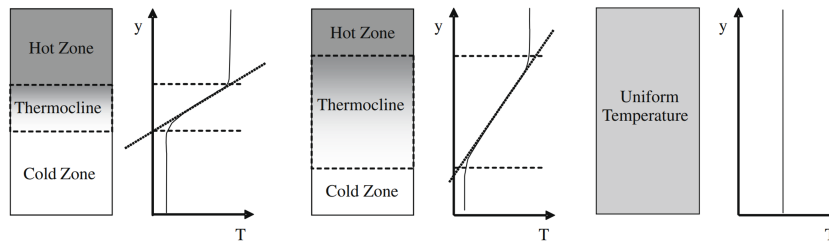
FIGURE 2.5: Thermal storage tank with varying degrees of stratification: highly stratified (left), moderately stratified (center) and fully mixed (right) [5]

systems are traditionally priced based on the total length of the heat exchangers installed, increasing the size of the borefield results in higher costs.

2.7.2 Short-Term Thermal Energy Storage Tanks

Short-term thermal energy storage tanks are designed to store thermal energy for durations ranging from a few hours to a few days. A stratified tank contains water that is divided into hot and cold zones, separated by a thermocline region. This separation into distinct hot and cold volumes facilitates more efficient use of the tank's thermal energy compared to a perfectly mixed tank. This is because the hottest water can be utilized for effective heating, and the coldest water for cooling, thereby maximizing the tank's efficiency [5]. Figure 2.5 illustrates different levels of tank stratification.

Domestic Hot Water Tank

In residential settings, short-term thermal energy storage tanks are commonly used for Domestic Hot Water (DHW) supply. These tanks help to reduce frequent cycling of heat pumps, which can lead to wear and lower the efficiency [35]. These problems

10

are addressed with hysteresis control of the heat pump. This system activates the heat pump when the tank temperature falls below a specified minimum level. The heat pump then charges the hot water tank until it reaches a preset temperature. The stored hot water can now be used to meet domestic hot water demands. When the tank hits its minimum temperature, the cycle starts again. The cycle repeats when the tank temperature drops again, ensuring a consistent hot water supply throughout the day and minimizing the need for the heat pump to frequently turn on and off [34]. Additionally, these tanks can store heat collected from solar thermal collectors (STCs) during daylight hours, enabling the use of renewable energy for domestic hot water needs during the evening and night [36].

Buffer Tank

Buffer tanks are used to manage the thermal storage for both heating and cooling systems, effectively limiting the required size of the heat source. Heat pumps and borefield heat exchangers are typically sized based on peak power demand. By using buffer tanks, the peak power demand can be reduced, which in turn allows for a smaller borefield and heat pump. The cost of installing a buffer tank is generally less than the cost savings achieved through component size reductions. Therefore, adding a buffer tank is beneficial to protect a heat pump or a borefield from fluctuating demand, such as the heating and cooling peaks in residential dwellings. The buffer tank absorbs short-term thermal peaks, thereby smoothing out fluctuations in demand by temporarily storing heat or cold [37].

2.8   Space Heating and Space Cooling Emission System

This section considers the emission system component to fulfill the space heating and cooling demand of the dwellings. In this thesis, the focus is solely on underfloor emission systems. In an underfloor heating or cooling system, a pipe network is installed beneath the floor. Hot or cold water circulates through this network, to heat or cool the space in the building. Underfloor emission systems enable heating and cooling with a small temperature difference between the water and the space for efficient heat exchange [14]. This is because the floor provides a large heat exchange area between the water in the pipes and the living space. Consequently, the heating demand can be met with a relatively low water supply temperature, while the cooling demand can be fulfilled with a relatively high water supply temperature.

2.9   District Heating Network

A district heating network is an interconnected piping system that links thermal instances such as heat generation and storage units to heat demand instances, like residential dwellings. Typically, this network is buried underground and uses a pump to transport water at a specific temperature as the heat carrier. In this thesis, a two-pipe residential district heating network is considered to connect dwellings with

a central borehole thermal energy storage unit. From the central storage unit, supply and return pipes at different temperatures extend to the residential district. The network functions as a collective heat source or sink, depending on whether the supply pipe contains hot or cold water. The pipes are insulated to avoid excessive heat losses to the surrounding ground. The dwellings are connected to the network via heat exchangers [29].

This thesis considers both 4th and 5th-generation residential district heating networks. The 4th generation network features a central heat generation unit, providing hot water to the network during heating season. The temperature of the water is sufficiently high for direct use in space heating within the dwellings. However, for domestic hot water needs, the temperature may be too low, requiring the installation of individual heaters. The primary advantage of the 4th-generation network is the cost reduction for the collective heat generation unit due to economies of scale. However, the high water temperature during the heating season requires the pipes to have adequate insulation. 5th generation district heating networks operate at near-ambient temperatures. This network serves as a low-temperature heat source for the dwellings, each of which requires a heat pump to upgrade the heat to usable temperatures for space heating and domestic hot water. Additionally, the network can function as a heat sink during the cooling season. In both scenarios, the 5th-generation network has minimal network losses due to the low operating temperatures. [29].

Chapter 3

System Selection

This chapter presents the residential energy systems that are modeled in Chapters 4 and 5 and investigated in Chapter 6. The systems are composed of the system components, which are introduced in Chapter 2, and all contain PV panels and STCs. The systems are designed in accordance with a set of system requirements, provided in Section 3.1, which specify the general framework within which the systems must operate. Subsequently, Section 3.2 discusses the system design process. Finally, Section 3.3 elaborates on the four selected systems.

3.1 System Requirements

The selected systems must provide space heating, cooling, domestic hot water, and electricity to a virtual district of 50 similar low-energy buildings with an underfloor emission system. The system is located in a Belgian climate and should meet the demand in a low-carbon manner. Therefore, all energy needs should be met by electricity from the grid connection or renewable solar energy through PV panels or STCs. It is assumed that the dwellings are located in an area with little open space. Therefore, a large central solar field is not possible, so the PV panels and STCs must be installed on the roof. The system is located in Belgium, where the demand for space heating and cooling is dominated by heat. The main focus of this thesis is to investigate how PV and STC perform in these systems. As a result, the systems should include these technologies. In order to make a fair comparison between them in the analysis, the systems must be designed to have a high degree of self-utilization of the generated PV and STC energy.

3.2 System Design Considerations

This section provides an overview of the common design considerations for the four selected systems. The following sections address these considerations by demand type, and one section is dedicated to collective seasonal thermal energy storage. In all systems, heating and cooling is provided by heat pumps. A heat pump is a

low-carbon heating solution and is preferred over electric resistance heating because it can perform both heating and cooling, and its COP is greater than one, meaning less electricity is needed to generate the same amount of heat.

3.2.1 Electricity

Every dwelling has its own grid connection, allowing electricity to be purchased to meet its electricity demand. To reduce reliance on electricity from the grid, each dwelling is equipped with a PV system, a home battery installation, and a hybrid inverter. The hybrid inverter manages the electricity flows between the PV panels, the battery, the total electrical demand of the dwelling, and the grid. These flows are managed to maximize the self-utilization of PV-generated electricity. This means that generated electricity first provides instantaneous demand. When the demand is saturated, it charges the battery. If the battery reaches its full capacity, excess electricity is fed into the grid. This excess is typically sold at a lower injection remuneration tariff than the grid electricity offtake cost. For the dwelling's electricity needs, the system prioritizes using electricity from the PV panels. If the PV-generated electricity is insufficient to meet the demand, the system then utilizes stored energy from the battery. If the combined PV and battery sources do not meet the dwelling's total electricity requirement, additional electricity is purchased from the grid at the prevailing offtake tariff.

Electricity is a very versatile energy carrier, capable of also supplying heating, cooling, and domestic hot water with the help of a heat pump. Since heat pumps are present in the system, and grid electricity is always available, the grid connection can meet all demands at all times, even in the absence of PV panels and/or STCs.

A community battery is an alternative to a home battery. Such a large central battery can be operated similarly to distributed home batteries, storing the surplus of generated PV electricity for later use. Community batteries typically achieve higher levels of self-utilization of PV electricity compared to a set of distributed home batteries with the same combined capacity. However, they are more complex to implement and are currently not preferred over home batteries [38, 39]. Therefore, they are not considered in this thesis, as the functionality of home batteries is very similar.

3.2.2 Seasonal Thermal Energy Storage

All four systems feature a collective seasonal thermal energy storage system that stores heat from cooling and STC, to use the stored heat during the heating season. This storage is connected to the residential dwellings via a district heating system. Hermans et al. [10] modeled and evaluated different collective seasonal thermal energy storage technologies for a residential district in Belgium with similar heating and cooling demands as in this work. They concluded that a low-temperature borefield with a buffer tank, combined with a fourth or fifth-generation district heating network, is a cost-effective solution. Therefore, a borefield with a buffer

14

tank is implemented in all four selected systems. Two of these systems incorporate a 4th-generation district heating network with a central heat pump, while the other two use a 5th-generation network with a central heat exchanger. The buffer tank reduces the size of the borefield by covering the district's demand peaks, thereby smoothing the load on the borefield [40].

No other forms of seasonal thermal energy storage for high-temperature heat from distributed STCs are considered, as the collectors are installed at the dwellings. A high-temperature pipe in the district heating network would be required to transport the heat from the distributed STCs, leading to higher losses. Therefore, high-temperature seasonal thermal energy storage has greater potential when combined with a central STC field, which is not considered in this thesis [29].

3.2.3 Domestic Hot Water

The residential dwellings are equipped with a Domestic Hot Water (DHW) tank to store heated water. Hot water is drawn directly from this tank to meet the DHW demand. Since DHW demand tends to be highly irregular, the tank serves as a reservoir, ready to fulfill the demand as needed. The water is heated using a residential heat pump powered by electricity. The heat source for the DHW heat pump can be either ambient air or the district heating network connected to the borefield.

When rooftop STCs are installed on each building, the heat generated is used to meet the DHW demand. STCs are an appropriate renewable energy source for DHW, as it is the main heat demand during summer when abundant solar energy is available [41]. The heat generated by the STC is injected into the DHW tank, similar to the heat pump. The DHW tank acts as a buffer, storing excess STC heat in the short term for later use. When both the instantaneous DHW demand and the DHW tank capacity are saturated, the STC injects the surplus heat into the district heating network. In this case, the STC exchanges heat at the network's temperature, which is lower than the temperature required for DHW. This allows the collectors to operate more efficiently than when generating DHW heat. Another situation in which STC heat is injected into the district heating network occurs when solar irradiation is insufficient to generate heat at a temperature high enough for DHW, but strong enough to generate heat for the district heating system. The type of collector used is the flat plate collector, selected because it is a popular and cost-effective choice for residential applications in this climate [34].

3.2.4 Space Heating

Space heating is provided by a heat pump that injects heat into the underfloor emission system. Heat pumps are an excellent choice for use with underfloor heating systems because they enable heating with a low supply temperature, which allows the heat pump to operate more efficiently at a higher COP. In the selected systems, either one large collective heat pump generates heat for the entire district, or smaller

15

individual heat pumps are installed in each dwelling, depending on the system configuration. Using solar thermal collectors as a heat source for space heating is avoided due to the seasonal mismatch between solar energy availability and heating demand, as well as the limited heating needs of low-energy buildings during periods of high solar gains. Therefore, STCs are not used for this purpose [41].

3.2.5 Cooling

Space cooling utilizes the same underfloor emission system as space heating. This system is capable of accommodating a relatively high water temperature. The primary cooling method in the selected systems is passive cooling, with the district heating network serving as a heat sink. In passive cooling, the network's temperature is sufficiently low to allow natural heat transfer from the cooled space to the network. When the network temperature is too high, natural heat transfer is insufficient, and active cooling is required. Active cooling involves actively extracting heat from the dwelling.

3.3 Selected Systems

This section discussed the final four concepts, referred to as 4Ga, 4Gb, 5Ga, and 5Gb, which are discussed in this order. Given the many similarities between the systems, the first system will be explained in more detail, while the other subsections will focus on highlighting the differences between the systems. The designations 4G and 5G represent the 4th and 5th generation district heating networks included in each system. The suffixes a and b indicate the difference in the low-temperature heat source of the DHW heat pump. The icons used in the system figures are shown in Table 3.1.
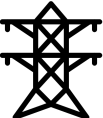
Electrical Grid	Hybrid Converter	Home Battery	Home Appliances	Underfloor Emission

TABLE 3.1: Component icons utilized in the system figures

3.3.1 System 4Ga

Figure 3.1 represents system 4Ga, with only one district building visible. The dwellings either inject or extract heat to the 4th generation district heating network via heat exchangers at node 1. This results in an aggregated heat load on the central thermal components. The district's demand on the borefield can either extract heat from or inject heat into the borefield. In the first case, cold water flows to the borefield to extract heat and transport it to the district via the hot pipe. This is referred to as the *heating mode* of the network, as shown in Figure 3.1a. In the second

16

(A) Heating mode

(B) Cooling mode
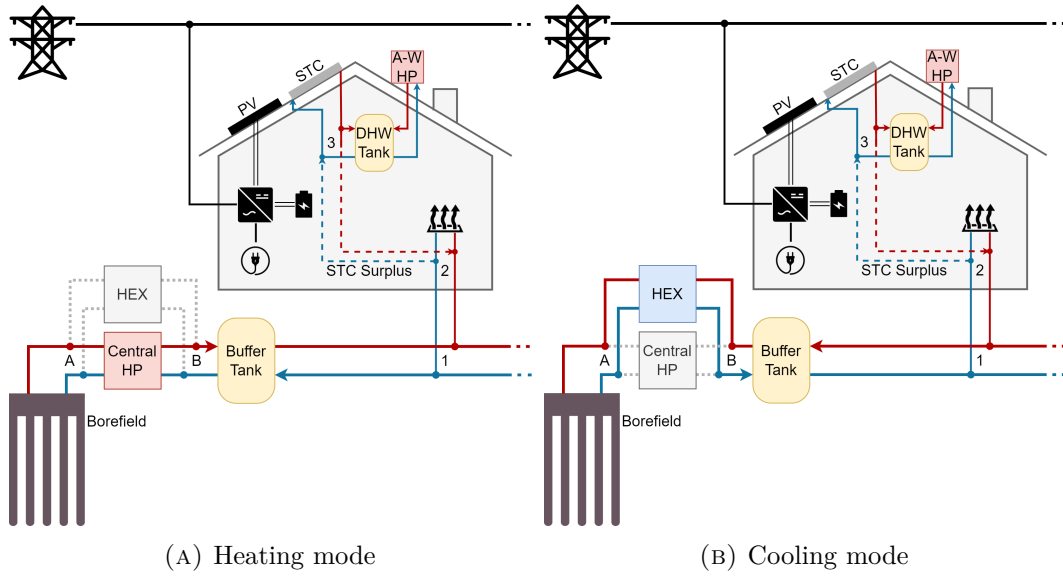
FIGURE 3.1: Schemes of system 4Ga in two modes applied on one dwelling of the district (PV: Photovoltaic Panel, STC: Solar Thermal Collector, DHW Tank: Domestic Hot Water Tank, A-W HP: Air-Water Heat Pump, Central HP: Central Heat Pump, HEX: Heat Exchanger)

case, the flows are reversed, allowing hot water to inject heat into the borefield. This is known as the *cooling mode*, represented in Figure 3.1b.

Regardless of the operation mode, the grid-connected PV-home battery installation supplies power to the dwelling's electricity demand. The installation is designed to maximize the self-consumption of PV-generated electricity and thus minimize the electricity needed from the grid.

The STCs operate independently of the district network's mode. They inject their heat into the DHW tank to reduce the need for auxiliary heating, which is provided by a hysteresis-controlled air-water heat pump. The STC heat surplus which is not used for DHW is redirected from node 3 to node 2.

In *heating mode*, the district heating network experiences a net aggregated heat flow from the borefield to the district. Dwellings extract heat from the network for space heating, while the central ground source heat pump extracts heat from the borefield and delivers it at a high temperature via the buffer tank to the heating network. This temperature is sufficient for the dwellings to use heat directly for space heating. Note that any STC surplus heat injected at node 2 while the dwellings extract heat is directly used for space heating.

In *cooling mode*, the heat flow in the district heating network is reversed. The district injects heat into the district heating network from space cooling and STC surplus heat. The heat then flows from the district to the buffer tank. A heat exchanger between nodes A and B, bypassing the central heat pump, directs heat from the buffer tank to the borefield to regenerate it. Passive cooling is replaced by active cooling with the central heat pump when the borefield temperature becomes too high.

3.3.2 System 4Gb

(A) Heating mode   (B) Cooling mode
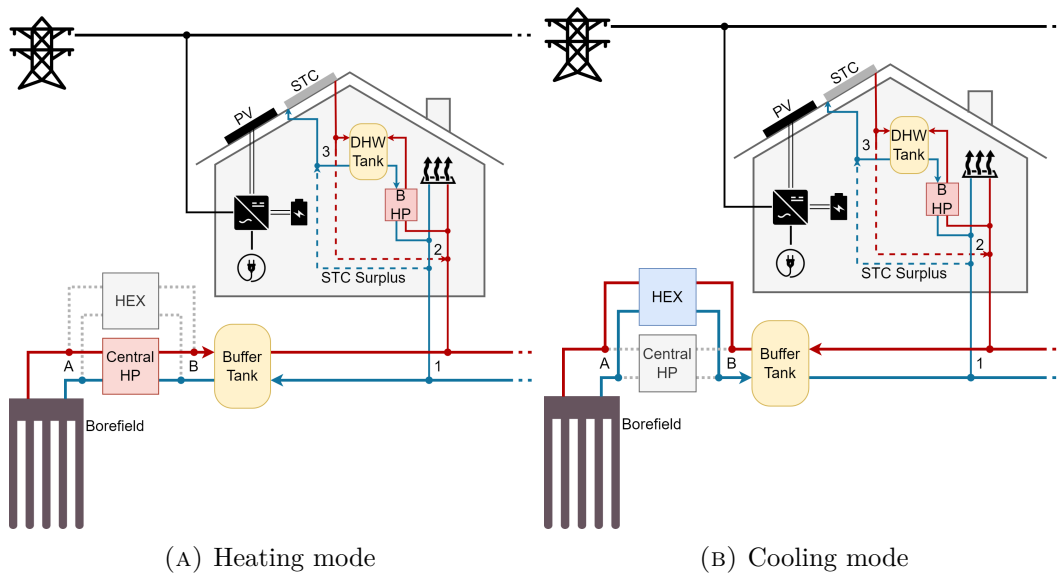
FIGURE 3.2: Schemes of system 4Gb in two modes applied on one dwelling of the district (PV: Photovoltaic Panel, STC: Solar Thermal Collector, DHW Tank: Domestic Hot Water Tank, B HP: Booster Heat Pump, Central HP: Central Heat Pump, HEX: Heat Exchanger)

System 4Gb is a district heating system similar to 4Ga, as depicted in Figure 3.2. The only difference is that a booster heat pump is used to generate DHW heat. The booster heat pump is a water-water heat pump that upgrades the heat available from the district heating network at node 2 to a temperature suitable for DHW. It is important to note that this booster heat pump adds an extra load to the collective district heating system, resulting in a need for larger component sizing. In particular, the borefield storage size is significantly increased, as it is now relatively more depleted by this additional heat demand without corresponding regeneration.

3.3.3 System 5Ga

Figure 3.3 depicts system 5Ga, which features a 5th-generation low-temperature district heating network. Each dwelling is equipped with its own residential water-water heat pump to provide space heating, utilizing the network as a low-temperature

(A) Heating mode

(B) Cooling mode
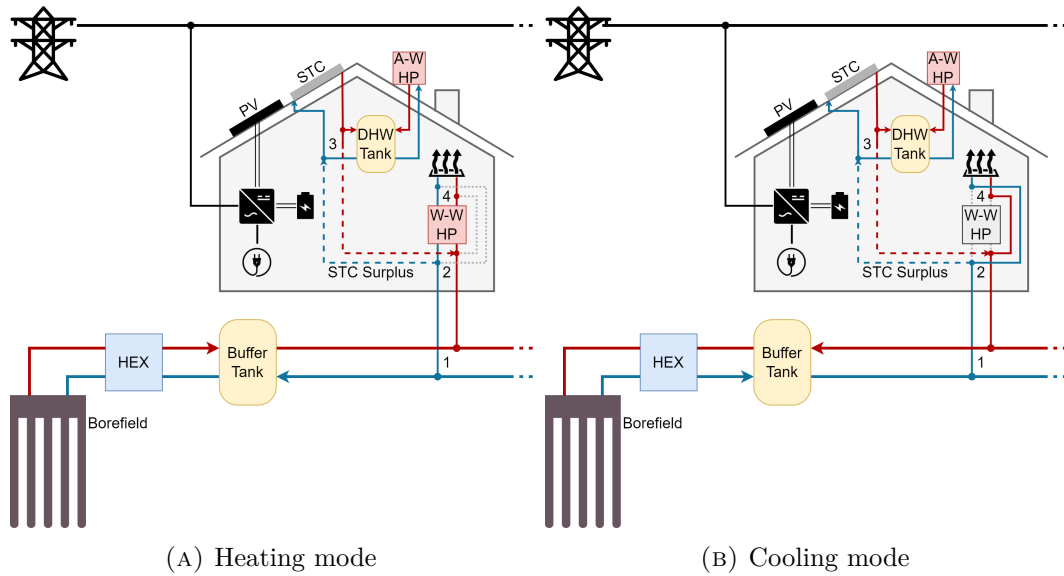
FIGURE 3.3: Schemes of system 5Ga in two modes applied on one dwelling of the district (PV: Photovoltaic Panel, STC: Solar Thermal Collector, DHW Tank: Domestic Hot Water Tank, A-W HP: Air-Water Heat Pump, W-W HP: Water-Water Heat Pump, HEX: Heat Exchanger)

heat source. For space cooling, the water-water heat pumps are bypassed using water pipes between nodes 2 and 4 to enable passive cooling. When the network temperature is too high, the residential water-water heat pump is used to provide active cooling.

The electricity and DHW in system 5Ga are supplied similarly to system 4Ga, which includes a PV home battery system and an air-water heat pump with STCs. An important note is that node 2 in this system typically operates at a lower temperature compared to the 4G systems due to the absence of the central heat pump. Consequently, the STC operates more efficiently when it injects its surplus heat at node 2 compared to operating in a 4th generation network.

3.3.4 System 5Gb

System 5Gb is similar to system 5Ga, with the exception of the DHW auxiliary heating. In the 5Gb version, DHW is heated by the residential water-water heat pump, which is originally installed for space heating and active cooling. The heat pump temporarily generates high-temperature heat when needed for DHW. Due to the higher temperature, the COP of the residential heat pump when generating DHW is lower than when it is used for space heating. Similarly to 4Gb, 5Gb has an altered heat demand on the collective thermal system compared to 5Ga, resulting in a larger borefield.

(A) Heating mode

(B) Cooling mode
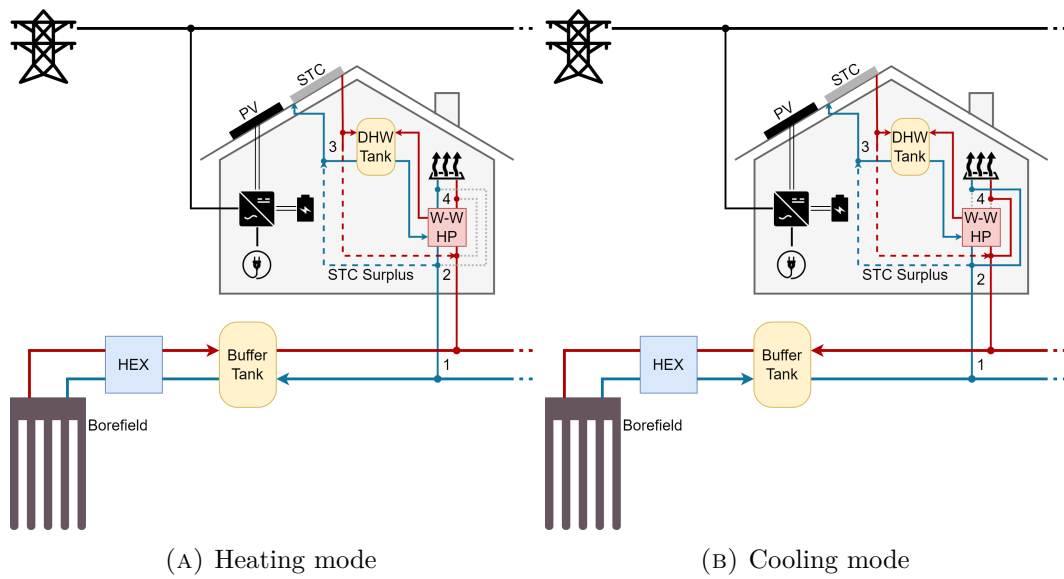
FIGURE 3.4: Schemes of system 5Gb in two modes applied on one dwelling of the district (PV: Photovoltaic Panel, STC: Solar Thermal Collector, DHW Tank: Domestic Hot Water Tank, B HP: Booster Heat Pump, W-W HP: Water-Water Heat Pump, HEX: Heat Exchanger)

Chapter 4

Model Approach

This chapter introduces the methodology used to model the selected systems from Chapter 3 and to determine the trade-off between PV panels and STCs. Section 4.1 provides a high-level overview of the model approach. Subsequently, the performance indicators used to quantify the panels in the modeled systems are explained in Section 4.2. Finally, the model input data, which defines the boundary conditions of the model, is discussed in Section 4.3.

4.1 Model Approach Overview

The systems are modeled by performing energy-flow calculations. The code for the model is developed in *Python* with the help of AI tools [42, 43]. The energy-flow calculations are performed with an hourly resolution, which is recommended to capture intraday fluctuations in demand and generation [7]. Each hour, electricity, heat, and cold are generated, converted, stored, and provided to the demand. The energy-flows are directed by rule-based controlled components. A synthetic hourly residential demand profile is plugged into the model, which performs the energy-flow calculations to supply the demand. The systems have components that should be sized adequately according to the demand profile to obtain a representative model. Once the energy flows and component sizes are known, the systems' operational CO_2 emissions and Total Cost of Ownership (TCO) can be determined. Both the CO_2 emissions and the TCO are calculated over a certain project lifetime of 40 years, a recommended period in this field of study [10].

To determine the trade-off between STC and PV panels on these emissions and costs, the energy-flow calculations are performed for different combinations of the number of rooftop STC and PV panels installed in the selected systems from Section 3.3. Assuming a max of 12 panels on each roof, there are 91 combinations of the number of STC and PV pairs when the same set of panels is installed on each building. The model iterates over these pairs and then calculates the CO_2 emissions and TCO for all the combinations.

4.2 Performance Indicators

Comparing PV panels and STCs can be challenging due to their distinct technologies, costs, efficiencies, and energy carriers. To provide a comprehensive comparison, it is advisable to use multiple performance indicators [44]. In this thesis, the performance of PV panels and STCs is evaluated from both economic and ecological perspectives. Economically, the total cost of ownership is used as the primary metric, while operational CO_2 emissions serve as the ecological metric. To ensure a nuanced comparison, the performance is assessed using these two key metrics.

4.2.1 Total Cost of Ownership

The cost of a system over its investment period is referred to as the Total Cost of Ownership (TCO). A system with a lower TCO, while supplying the same demand, is considered more cost-effective. In this thesis, the TCO of a system is composed of its Investment Cost (IC) and its Operational Cost (OC):

$$TCO = IC + OC \tag{4.1}$$

The IC of the system represents the total investments in system components during the investment period. Typically, these component investments occur at the beginning of the first year of the investment period. Components may have a shorter lifespan than the investment period and thus require replacement. These later reinvestments are actualized to the first year using an annual discount rate r. The system's investment cost, composed of individual component investment costs $IC_{component,t}$ in year t, is given by:

$$IC = \sum_{component}^{system} \sum_{t=0}^{period-1} \frac{IC_{component,t}}{(1+r)^t} \tag{4.2}$$

The system's OC includes Maintenance Costs (MC) and grid Electricity Costs (EC). These are annual expenditures occurring at the end of each year t and are also actualized to the first year. Thus, the system's OC during its investment period is:

$$OC = \sum_{t=1}^{period} \frac{MC_t + EC_t}{(1+r)^t} \tag{4.3}$$

The investment period is considered equal to the project lifetime of 40 years and an annual discount rate of 5% is used according to [45]. The relevant cost data for the components used in the TCO calculations are provided in Table A.1. Some components need to be sized to determine their IC and MC, with MC considered a fraction of IC. This component sizing is discussed in Chapter 5. A constant electricity offtake tariff of €0.30/kWh is assumed, and a Belgian feed-in remuneration of €0.045/kWh is considered according to [46].

4.2.2 Carbon Dioxide Emissions

Since the selected systems are low-carbon residential energy systems that do not rely on fossil fuels for heating, the carbon content of the grid electricity is the sole source of operational CO_2 emissions. In this analysis, the ecological performance of a system is evaluated based exclusively on its operational CO_2 emissions. Other sources of CO_2 emissions, such as those from manufacturing or end-of-life processes, are beyond the scope of this thesis.

In the model, electricity is drawn from the grid by the central heat pump, as well as by individual dwellings to power electric home appliances and residential heat pumps. Details on how the grid demand is calculated are provided in Sections 5.7 and 5.9. A constant carbon intensity of 127 CO_2-eq/kWh, representing the average carbon intensity in Belgium [7], is used. With this carbon intensity and the electric grid demand, the annual CO_2 emissions can be calculated.

4.3 Model Input Data

The input data for the system models includes residential energy demand profiles for domestic hot water, heating, cooling, and electricity. As detailed in Section 3.1, the energy system has to provide a virtual district of 50 identical low-energy buildings in Belgium. Each dwelling is assumed to have a total heated and cooled floor area of 150 m^2. The annual energy requirements for each building are specified as follows: 30 kWh/m^2 for space heating, 10 kWh/m^2 for space cooling, and 6.27 kWh per day for domestic hot water [10]. The electricity consumption for household appliances is assumed to be 3500 kWh annually, which is typical for a Belgian household [47]. Synthetic hourly load profiles for these newly built residential buildings in Belgium are generated for a full year using the nPro tool. This tool creates profiles based on normalized demand profiles for the building type [48].

Figure 4.1 illustrates the evolution of the generated profiles for space heating and cooling, showing a clear distinction between the heating and cooling seasons. Both demands are plotted positively for clarity, even though the physical heat flows occur in opposite directions. Figures 4.2 and 4.3 respectively display the synthetic domestic hot water and electricity demand profiles for a single dwelling. Unlike space heating and cooling, these loads are consistent throughout the year with minor seasonal variations. The annual demand and peak power for each demand profile for one building are summarized in Table 4.1. Given that the district comprises 50 identical buildings, the same demand profiles are applied to each building.

In addition to the demand profiles, the model incorporates other profiles related to the energy system's geographical location, situated in Belgium. First, the ambient air temperature profile of a typical Belgian year, provided by the API of Open-Meteo, is shown in Figure 4.4. This temperature profile is essential for accurately modeling the performance of the heat pumps and other temperature-dependent components.
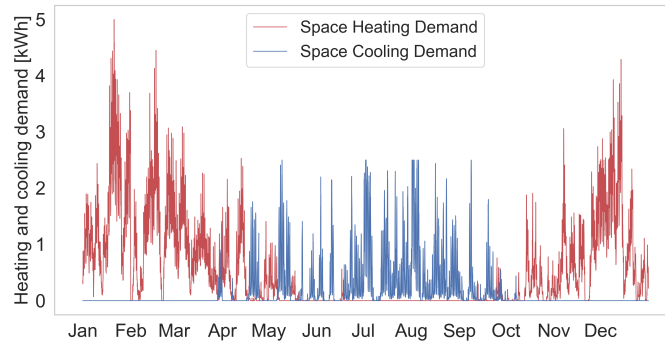
FIGURE 4.1: Domestic hot water demand profile of a single dwelling
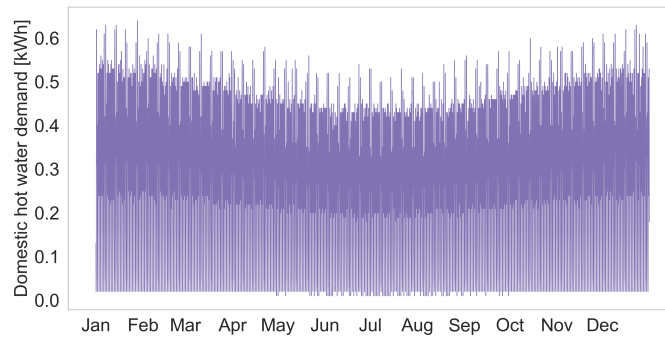
FIGURE 4.2: Domestic hot water demand profile of a single dwelling
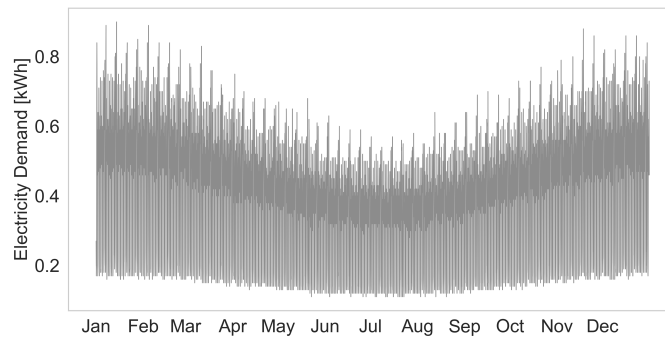
FIGURE 4.3: Electricity demand profile for household appliances of a single dwelling

Demand Type	Annual Demand [kWh]	Peak Demand [kW]
Electricity	3500	0.9
Domestic Hot Water	2290	0.6
Space Heating	4500	5.0
Space Cooling	1500	2.5

TABLE 4.1: Demand characteristics for a single dwelling
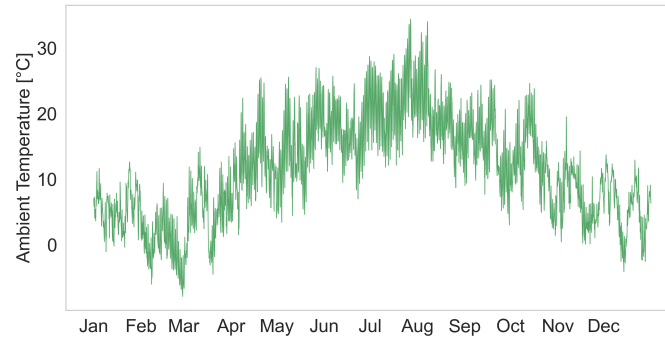
FIGURE 4.4: Ambient temperature profile for a Belgian climate
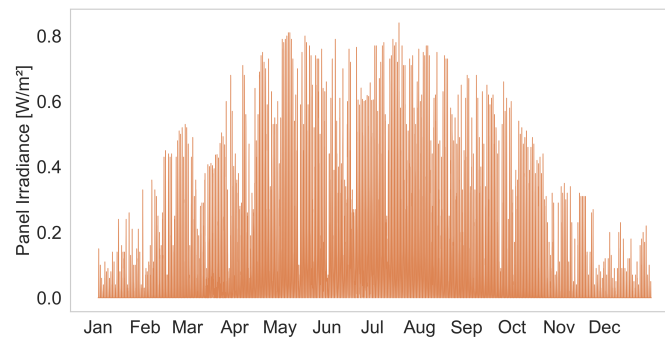
FIGURE 4.5: Solar irradiance profile on a 35° inclined southwards panel in Belgium

Next, solar irradiance is needed to calculate the STC and PV energy generation. For optimal solar exposure, the panels are positioned facing south with an elevation angle of 35°, which maximizes solar irradiance per square meter [27]. The evolution of solar irradiance on such a tilted panel in Belgium is depicted in Figure 4.5, corresponding to a total annual irradiation of 921 kWh/m^2. Finally, Figure 4.6 presents a temperature profile of PV panels installed on a gable roof, measured at EnergyVille in Genk. This profile is used to assess the efficiency of the PV panels under typical Belgian weather conditions.
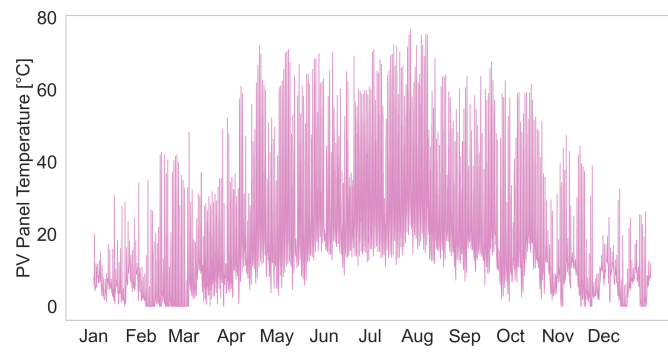
FIGURE 4.6: Temperature profile of a rooftop PV panel in Belgium

Chapter 5

Component Models

This chapter presents the implementation of the system components within the hourly energy flow model. The components are discussed sequentially, in the order they appear in the model. Each section explains the modeling of a component by addressing the following aspects: First, the general equations that describe the energy flows to and from other components each hour are presented. Subsequently, the component parameters considered in the model to specify the general equations, are introduced.

5.1 Domestic Hot Water Tank

All four systems include a DHW tank that temporarily stores hot water to buffer the intermittent production of the Solar Thermal Collectors (STC) and the auxiliary heat pump. This ensures a continuous hot water supply without requiring these heat generation units to meet the demand instantly.

5.1.1 General Equations

The tank is modeled as a perfectly mixed tank with a uniform water temperature. The general equation for the domestic hot water energy content $Q_{tank,i}^{dhw}$ [Wh] with tank volume V_{tank}^{dhw} [m^3] at hour i is:

$$Q_{tank,i}^{dhw} = \rho_w \cdot c_{p,w} \cdot V_{tank}^{dhw} \cdot \left(T_{tank,i}^{dhw} - T_{tank,min}^{dhw} \right) \tag{5.1}$$

where ρ_w [kg/m^3] is the density of water, $c_{p,w}$ [J/(kg $\cdot$ K)] is the specific heat capacity, $T_{tank,i}^{dhw}$ [°C] is the current tank temperature, and $T_{tank,min}^{dhw}$ [°C] is the minimum tank temperature. Given the energy content of the tank, at hour i, the energy content of the tank in the next hour is calculated by the following equation:

$$Q_{tank,i+1}^{dhw} = Q_{tank,i}^{dhw} - Q_{tank,loss}^{dhw} - Q_{demand,i}^{dhw} + Q_{stc,i}^{dhw} + Q_{hp,i}^{dhw} \tag{5.2}$$

Here is $Q_{tank,loss}^{dhw}$ [Wh] the fixed hourly heat losses, and $Q_{demand,i}^{dhw}$ [Wh], $Q_{stc,i}^{dhw}$ [Wh] and $Q_{hp,i}^{dhw}$ [Wh] correspond respectively to the hourly hot water demand, the STC

heat gain, and the heat from the auxiliary heat pump. The hot water demand at hour i is known by the demand profile.

The domestic hot water tank operates between a maximum and minimum water temperature. The maximum tank temperature is set at 60°C because higher temperatures significantly reduce the efficiency of the STC in generating domestic hot water heat, according to [34]. The heat pump switches on when the tank temperature reaches the minimum of 39°C, a typical temperature at which DHW is used [49]. The heat pump is then assumed to reheat the tank until it reaches 49°C, after which the heat pump switches off.

5.1.2 Component Parameters

The Daikin EKHWS type 300D3V3 tank data in Table 5.1 is considered for specific data on the domestic hot water tank. This is a standard residential tank for domestic hot water with the option to connect STC [8]. The 292 l version is chosen according to guidelines for domestic hot water tanks with STC for an average household [34]. This tank with a fixed tank size is chosen for all systems, and its investment cost per unit is given in Table A.1

DHW Tank	
V_{tank}^{dhw} [m³]	0.292
$Q_{tank,loss}^{dhw}$ [W]	68

TABLE 5.1: Technical data of the domestic hot water tank [8]

5.2 Solar Thermal Collectors

The solar thermal collectors are used in all the systems as a renewable energy source for generating heat from solar irradiation. The energy flows of each system are calculated for all possible combinations of rooftop STCs and PV panels, with a maximum of 12 panels.

5.2.1 General Equations

The general equations of the STC, introduced in Section 2.5, are now applied on an hourly basis. The equation for the heat gain $Q_{stc,i}$ [Wh] in hour i of n_{stc} installed STCs, each with an aperture area $A_{stc,a}$ [m²], is:

$$Q_{stc,i} = \eta_{stc,i} \cdot G_i \cdot A_{stc,a} \cdot n_{stc} \tag{5.3}$$

Here is $\eta_{stc,i}$ the hourly STC efficiency, and G_i [Wh/m²] hourly the solar irradiation. The solar irradiation is determined by the given hourly profile of a Belgian year for a southwards panel with an inclination of 35°. The efficiency of a single STC is

calculated using the following equation:

$$\eta_{stc,i} = \eta_0 - k_1 \frac{T_{stc,i}^{fluid} - T_{amb,i}}{G_i} - k_2 \frac{\left(T_{stc,i}^{fluid} - T_{amb,i}\right)^2}{G_i} \qquad (5.4)$$

where the optical efficiency η_0, which is the maximum efficiency, and the effective heat loss coefficients k_1 [W/m$^2 \cdot$ K] and k_2 [W/m$^2 \cdot$ K^2] are technical characteristics of a specific collector. The hourly ambient air temperature, $T_{amb,i}$ [K], and the solar irradiance are available from profiles with an hourly resolution. The average STC fluid temperature, $T_{stc,i}^{fluid}$ [K], is considered to be the average of the inlet temperature, $T_{stc,i}^{in}$ [K], and the outlet temperature, $T_{stc,i}^{out}$ [K], at hour i:

$$T_{stc,i}^{fluid} = \frac{T_{stc,i}^{in} + T_{stc,i}^{out}}{2} \qquad (5.5)$$

When collectors are connected in series, the first collector's output temperature becomes the second collector's input temperature. This change results in the second collector operating at a lower efficiency, as its average fluid temperature is higher. Consequently, the overall efficiency of the solar installation decreases with each additional collector connected in series. Although series-connected STCs can achieve very high outlet temperatures for the last collector, in the model, multiple collectors are considered to be connected in parallel. This parallel configuration maintains higher efficiency, as the outlet temperatures required for domestic hot water are relatively low. The disadvantage of parallel installation is that series-connected STCs potentially generate useful heat when solar irradiation is insufficient for a parallel installation to generate heat useful heat.

A common approach to controlling solar thermal collectors is to maintain a fixed temperature difference of 10 K between each collector's inlet, $T_{stc,i}^{in}$ [°C] and outlet, $T_{stc,i}^{out}$ [°C], temperatures by adjusting the volume flow rate of the working fluid [50]. Since identical STCs are connected in parallel, the temperature difference across each collector remains the same. However, the total flow rate is divided among the individual collectors. Therefore, in hour i, the volume of fluid $V_{stc,i}^{fluid}$ [m^3] flowing through a single STC of n_{stc} parallel-installed collectors is given by:

$$V_{stc,i}^{fluid} = \frac{Q_{stc,i}}{n_{stc} \cdot \rho_{stc} \cdot c_{p,stc} \cdot \left(T_{stc,i}^{out} - T_{stc,i}^{in}\right)} \qquad (5.6)$$

$$= \frac{Q_{stc,i}}{n_{stc} \cdot \rho_{stc} \cdot c_{p,stc} \cdot 10 \text{ K}} \qquad (5.7)$$

In this equation, ρ_{stc} [kg/m^3] and $c_{p,stc}$ [J/(kg·K)] are the density and the isobaric specific heat capacity of the STC working fluid. The formula clearly indicates that the flow rate is scaled with the heat gain to maintain a constant temperature increase of 10 K over the installation. However, the range of optional hourly flows is limited by a maximum and a minimum value. These limits are determined by the minimum flow rate $\dot{V}_{stc,min}^{fluid}$ [m^3/s] and a maximum flow rate $\dot{V}_{stc,max}^{fluid}$ [m^3/s] for a specific collector. These flow limits should be considered when determining the heat gain.

STC Heat Gain Allocation

The primary goal of the STCs is to charge the domestic hot water tank. However, when the DHW tank is fully charged, the surplus heat is redirected to the district heating network, which is their secondary goal. Additionally, when the STCs are unable to generate high-temperature heat for DHW due to insufficient solar power, the STC will generate lower-temperature heat for the district heating network. The next two sections discuss the steps taken in the model to determine what portion of the heat generated by the STCS is used to cover DHW demand, $Q_{stc,i}^{dhw}$ [Wh], and what portion is transferred to the network, $Q_{stc,i}^{dhn}$ [Wh].

Solar Thermal Collector Heat Gain For Domestic Hot Water

To determine $Q_{stc,i}^{dhw}$, the model first checks the available capacity in the DHW tank after accounting for tank losses and DHW demand in hour i. This charging potential of the DHW tank is expected to be greater than zero since tank losses occur every hour. Next, the model sets the inlet temperature of the STCs equal to the current DHW tank temperature $T_{tank,i}^{dhw}$. By combining Equations (5.3), (5.4) and (5.5), the hourly potential heat gain from the STCs, $Q_{stc,pot,i}^{dhw}$ [Wh], at a fixed 10 K temperature difference is calculated. The corresponding flow rate $\dot{V}_{stc,i}^{fluid,dhw}$ [m³/s] is determined by converting the hourly volume from Equation (5.7) to a flow rate. Table 5.2 shows the determination of the actual generated DHW heat based on the flow rate, which is further explained in the following bullet points.

Collector fluid flow rate		DHW heat gain
$\dot{V}_{stc,i}^{fluid,dhw} \in \left[\dot{V}_{stc,min}^{fluid}, \dot{V}_{stc,max}^{fluid} \right]$	$\Rightarrow$	$Q_{stc,i}^{dhw} = f_i \cdot Q_{stc,pot,i}^{dhw}$
$\dot{V}_{stc,i}^{fluid,dhw} > \dot{V}_{stc,max}^{fluid}$	$\Rightarrow$	$Q_{stc,i}^{dhw} = f_i \cdot Q_{stc,pot,i}^{*dhw}$
$\dot{V}_{stc,i}^{fluid,dhw} < \dot{V}_{stc,min}^{fluid}$	$\Rightarrow$	$Q_{stc,i}^{dhw} = 0$

TABLE 5.2: Determination of solar thermal collector heat generation for domestic hot water $Q_{stc,i}^{dhw}$ [Wh] based on working fluid flow rate $\dot{V}_{stc,i}^{fluid,dhw}$ [m³/s]

- If the volume flow rate is within the physical range, the potential STC heat is transferred to the DHW tank during fraction f_i of the hour. The fraction corresponds to the part of the potential heat gain that can be injected into the DHW without exceeding its maximum energy content.

- In case the calculated STC fluid flow rate exceeds its maximum, determined by the manufacturer, the temperature difference over the STC is adjusted to obtain the maximum fluid flow rate. Now Equation (5.7) is not valid anymore, and an algebraic loop arises: The outlet temperature becomes dependent on the efficiency, which in its turn is dependent on the outlet temperature. This algebraic loop is solved analytically after combining Equations (5.3), (5.4),

(5.5) and (5.6) to a quadratic equation in $T_{stc,i}^{out}$. The solution corresponds to an adjusted potential STC heat generation for domestic hot water, $Q_{stc,pot,i}^{*dhw}$ [Wh], with the STC operating at the maximum flow rate with the increased inlet-outlet temperature difference. From this adjusted potential, again, an adequate fraction of f_i is injected into the tank depending on the current tank charge.

- When the calculated volume flow rate is lower than the minimum, the model considers that no STC heat is used for domestic hot water, and this $f_i = 0$. This opens up the opportunity to generate heat for the network.

Solar Thermal Collector Heat Gain For District Heating Network

The collectors generate heat for the district heating network $Q_{stc,i}^{dhn}$ when the collectors generate excess DHW heat or when the STCs do not generate DHW heat due to too low work fluid flow rate. The approach is similar to the previous section. The model first calculates the potential heat gain for the network $Q_{stc,pot,i}^{dhn}$ [Wh] and the corresponding flow rate $\dot{V}_{stc,i}^{fluid,dhn}$ [m³/s] with the 10 K STC temperature difference. However, the inlet temperature is now set at the water temperature of the cold pipe of the district heating network $T_{cold,i}^{dhn}$, altered with 2 K to consider the temperature drop of the heat exchanger. Next, the model determines the heat gain for the network based on how the volume flow rate of the STC work fluid relates to the physically possible range, as summarized in Table 5.3

Collector fluid flow rate		District network heat gain
$\dot{V}_{stc,i}^{fluid,dhn} \in \left[\dot{V}_{stc,min}^{fluid}, \dot{V}_{stc,max}^{fluid}\right]$	$\Rightarrow$	$Q_{stc,i}^{dhn} = (1 - f_i) \cdot Q_{stc,pot,i}^{dhn}$
$\dot{V}_{stc,i}^{fluid,dhn} > \dot{V}_{stc,max}^{fluid}$	$\Rightarrow$	$Q_{stc,i}^{dhn} = (1 - f_i) \cdot Q_{stc,pot,i}^{*dhn}$
$\dot{V}_{stc,i}^{fluid,dhn} < \dot{V}_{stc,min}^{fluid}$	$\Rightarrow$	$Q_{stc,i}^{dhn} = 0$

TABLE 5.3: Determination of solar thermal collector heat generation for district heating network $Q_{stc,i}^{dhn}$ [Wh] based on working fluid flow rate $\dot{V}_{stc,i}^{fluid,dhn}$ [m³/s]

- When the flow rate fits the range, the potential generated heat is injected into the district heating network during the complement fraction $1 - f_i$ of the hour i. Here f_i is the hourly fraction of potential domestic hot water heat sent to the hot water tank, as determined in the previous section.

- If the calculated STC work fluid flow rate exceeds its maximum value, an adjusted potential heat gain for the district heating network, $Q_{stc,pot,i}^{*dhn}$ [Wh], is determined analog to the previous section. Again, the complement fraction $1 - f_i$ of this adjusted potential heat generation is directed to the hot network pipe.

- In case the calculated volume flow rate is lower than the minimum, the STC cannot generate heat for the district heating network while maintaining the fixed STC temperature difference of 10 K. Therefore, the model considers no heat generation for the network.

5.2.2   Component Parameters

To solve the STC heat generation equations in Section 5.2.1, numerical values for $A_{stc,a}$, η_0, k_1, k_2, ρ_{stc} and $c_{p,stc}$ are required. These are characteristics of the considered solar thermal collector and its working fluid. Also, $\dot{V}_{stc,max}^{fluid}$ and $\dot{V}_{stc,min}^{fluid}$ of the selected collector is needed to determine the operating modes from Section 5.2.1. For this data the Logasol SKN 4.0-s flat plate collector and a water-glycol mixture working fluid is selected [9, 10]. The numerical values of the collector and the fluid are shown in Table 5.4. The investment cost of one solar thermal collector is given in Table A.1.

Flat plate collector	
$A_{stc,a}$ [m^2]	2.25
η_0	0.77
k_1 [W/(m$^2 \cdot$ K)]	3.22
k_2 [W/(m$^2 \cdot$ K^2)]	0.015
$\dot{V}_{stc,max}^{fluid}$ [m^3/s]	1.39 $\times 10^{-6}$
$\dot{V}_{stc,min}^{fluid}$ [m^3/s]	3.47 $\times 10^{-6}$
Water-glycol mixture	
ρ_{stc} [kg/m^3]	1070
$c_{p,stc}$ [J/kg $\cdot$ K]	3600

TABLE 5.4: Technical data of the flat plate solar thermal collector and its working fluid [9, 10]

5.3   Auxillary Domestic Hot Water Heat Pumps

The auxiliary domestic hot water heat pumps generate heat for the domestic hot water tank while extracting heat from a low-temperature heat source. All systems have an auxiliary hot water heat pump, but the type of unit varies between the systems.

5.3.1   General Equations

Using Equation (2.5), the heat generated by a heat pump for domestic hot water, $Q_{hp,i}^{dhw}$ [Wh], can be written for each hour i as:

$$Q_{hp,i}^{dhw} = COP_i^{dhw} \cdot W_{hp,i}^{dhw} \tag{5.8}$$

In this general equation, COP_i^{dhw} and $W_{hp,i}^{dhw}$ [Wh] are, respectively, the hourly coefficient of performance and the electricity consumption of the heat pump. The temperatures of the heat source and the heat sink influence COP_i^{dhw}. Because the heat is supplied at a fixed temperature, the model considers the COP_i^{dhw} temperature dependent only on the low-temperature heat source $T_{hp,i}^{source,dhw}$ [°C] with a linear relationship:

$$COP_i^{dhw} = a_{hp}^{dhw} \cdot T_{hp,i}^{source,dhw} + b_{hp}^{dhw} \tag{5.9}$$

with a_{hp}^{dhw} and b_{hp}^{dhw} fixed positive coefficients characterizing the behaviour of a specific heat pump. These coefficients are determined by linearly interpolating between pairs of COP^{dhw} and $T_{hp}^{source,dhw}$ as indicated on the heat pump's datasheet. For the DHW heat pumps, these pairs are specified for a fixed high-temperature supply of 55°C. Note that the COP is underestimated since no temperature dependency of the supply temperature is modeled and the 55°C is not always necessary to reheat the tank. Equation (5.10) defines the hourly heat load on the district heating network $Q_{hp:dhw,i}^{dhn}$ [Wh] by the heat pump, in case the heat pump uses the network as a heat source.

$$Q_{hp:dhw,i}^{dhn} = W_{hp,i}^{dhw} - Q_{hp,i}^{dhw} \tag{5.10}$$

5.3.2 Component Parameters

Depending on the modeled energy system, a different type of auxiliary domestic hot water heat pump has to be included. The difference lies in the low-temperature heat source. The three types of DHW heat pumps are: the air-water DHW heat pump, the Booster DHW heat pump, and the residential water-water heat pump used for DHW. To model these heat pumps, the data of respectively the Daikin Altherma M HW HHE260PCV37, NIBE Micro booster MT-MB21, and the Vitocal 200-G BWC from Viessmann are used. The COP curve coefficients derived from their data sheets are given in Table 5.5.

Heat Pump Type	a_{hp}^{dhw}	b_{hp}^{dhw}
Air-Water DHW HP	0.03	3.17
Booster DHW HP	0.047	4.13
Residential W-W HP (DHW)	0.08	2.62

TABLE 5.5: Linear interpolated COP curve coefficients of the heat pumps for domestic hot water [11, 12, 13]

The source temperature for the air-water DHW HP, $T_{amb,i}$ in °C, is known from the given hourly ambient temperature profile. The booster HP and the residential water-water HP use the hot pipe from the district heating network with temperature $T_{hot,i}^{dhn}$ [°C] minus 2°C as source temperature. The subtracted 2°C accounts for the heat exchanger between the dwelling and the district heating network.

The 1.82 kW air-water DHW HP and the 2.1 kW booster DHW HP are standard residential units. Therefore they are not sized, and a fixed cost per unit is considered,

displayed in Table A.1 [11, 12]. These heat pumps also have an integrated water tank of 240 l and 190 l, respectively. However, the model considers the dynamics of the DHW tank selected in Section 5.1 instead to ensure consistent behavior of the solar thermal collectors since they are important in the thesis. The sizing and the cost of the residential water-water HP are discussed in Section 5.4.2.

5.4 Residential Water-Water Heat Pump for Space Heating and Cooling

Systems 5Ga and 5Gb include a residential water-water heat pump for space heating and active cooling through an underfloor emission system. The heat pump utilizes the district heating network as a low-temperature heat source for heating and as a high-temperature heat sink for cooling.

5.4.1 General Equations

The dwellings are primarily passively cooled with a heat exchanger. Active cooling with the heat pump is only required when the temperature of the heat sink, $T_{hp,i}^{sink,sc}$ [°C], exceeds a specified limit. This maximum temperature is set at 18°C for an underfloor emission system, as defined in Section 3.1. Therefore, the following equations can be written to model the residential heat pump behavior for heating and cooling:

$$Q_{hp,i}^{sh} = COP_i^{sh} \cdot W_{hp,i}^{sh} \tag{5.11}$$

$$Q_{hp,i}^{sc} = COP_R^{sc} \cdot W_{hp,i}^{sc} \quad \text{for } T_{hp,i}^{sink,sc} > 18°\text{C} \tag{5.12}$$

Here, $Q_{hp,i}^{sh}$ [Wh] represents the heating, and $Q_{hp,i}^{sc}$ [Wh] represents the cooling, corresponding to their respective electricity needs $W_{hp,i}^{sh}$ [Wh] and $W_{hp,i}^{sc}$ [Wh] in hour i. The heating and cooling energy requirements are defined by the given hourly demand profiles. To determine the electricity needs, the coefficients of performance of the heat pump for heating and cooling, COP_i^{sh} and COP_R^{sc} and $T_{hp,i}^{sink,sc}$ are yet to be found. The hourly heat flows from and to the district heating network $Q_{hp:sh,i}^{dhn}$ (heating) and $Q_{hp:sc,i}^{dhn}$ (active cooling) are determined as:

$$Q_{hp:sh,i}^{dhn} = W_{hp,i}^{sh} - Q_{hp,i}^{sh} \tag{5.13}$$

$$Q_{hp:sc,i}^{dhn} = W_{hp,i}^{sc} + Q_{hp,i}^{sc} \tag{5.14}$$

5.4.2 Component Parameters

The performance coefficient for space heating, COP_i^{sh}, is determined similarly to the method used for the domestic hot water heat pump in the previous section, using Equation (5.9). The heat source temperature is again $T_{hot,i}^{dhn}$ [°C] minus 2 °C to account for the heat exchanger. The coefficients for the selected Vitocal 200-G BWC heat pump are provided in Table 5.6. This time, the coefficients are determined for a

heat pump outlet temperature of 35°C, which is an appropriate supply temperature for underfloor heating, as stated in Section 3.1.

Residential W-W HP (SH)	
a_{hp}^{sh}	0.14
b_{hp}^{sh}	4.63

TABLE 5.6: Linear interpolated COP curve coefficients of the residential water-water heat pump for space heating [13]

For the refrigeration coefficient of performance COP_R^{sc}, a constant value of 5.9 is considered [13]. The model checks each hour i to see if the heat sink temperature exceeds 18°C, which requires the heat pump to provide active cooling. If the temperature does not exceed this limit, passive cooling is provided by a heat exchanger. The heat sink temperature is equal to the temperature of the cold network pipe $T_{cold,i}^{dhn}$ [°C] plus 2°C, accounting for the heat exchanger between the residential heat pump and the water in the cold pipe.

To determine the investment cost of the heat pump, it is sized based on the hourly peak load in kW for the heat demand. The investment cost is calculated using the linear cost function shown in Table A.1. In system 5Ga, the peak load of the heat demand is defined by the maximum value in the hourly demand profile for space heating. In system 5Gb, however, the residential heat pump is also used for domestic hot water generation. Now, the instantaneous peak of the combined load for domestic hot water and space heating is considered.

5.5 District Heating Network

The district heating network allows heat flow between the central buffer tank and the district's dwellings. The section aims to transform the load profiles of the buildings to the aggregated load profile that is applied to the buffer tank. The process involves two primary steps: first, determining the combined aggregated profile of the dwellings, and second, calculating the network heat losses associated with this profile to define the load on the buffer tank. Finally, a section is added that includes a summary of the numerical values used in the model.

5.5.1 General Equations

District Heating Network Load

In the preceding sections of this chapter, various heat loads from individual buildings to their district heating network connections have been defined. Therefore, the total load $Q_{dwelling,i}^{dhn}$ [Wh] in hour i of a building in any of the four systems can be

determined by summing all possible contributions:

$$Q_{dwelling,i}^{dhn} = Q_{hp:dhw,i}^{dhn} + Q_{hp:sh,i}^{dhn} + Q_{4G:sh,i}^{dhn} + Q_{passive:sc,i}^{dhn} + Q_{hp:sc,i}^{dhn} + Q_{stc,i}^{dhn} \quad (5.15)$$

where the contributions can be zero or non-zero, depending on whether the components are installed and active. Loads $Q_{hp:dhw,i}^{dhn}$ [Wh], $Q_{hp:sh,i}^{dhn}$ [Wh], $Q_{hp:sc,i}^{dhn}$ [Wh] and $Q_{stc,i}^{dhn}$ [Wh] are dependent on the DHN temperature as explained in the previous sections. $Q_{4G:sh,i}^{dhn}$ [Wh] and $Q_{passive:sc,i}^{dhn}$ [Wh] represent the space heating load for a fourth-generation network and the passive cooling load of the dwelling, respectively. Both are determined by the hourly demand profiles and can be met by directly using heat from the DHN without the need for a heat pump.

An aggregated load profile, $Q_{aggregated,i}^{dhn}$ [Wh], of the district from a single dwelling's load is obtained using a diversity factor. This factor accounts for the temporal dispersion of demand peaks among individual consumers, effectively reducing the peak power of the aggregated profile. For a district of 50 buildings with similar demand patterns, a diversity factor of 0.75 is recommended [51], which reduces the peak load of the aggregated profile by 25% while maintaining the total energy volume. It is important to note that the peak generation from solar thermal collectors is not reduced by this factor, as excessive solar radiation affects all buildings similarly, resulting in a common peak power. By combining the aggregated load profile and the heat losses of the district heating network, $Q_{loss,i}^{dhn}$ [Wh], the district load on the collective central components, $Q_{district,i}^{dhn}$ [Wh], is defined:

$$Q_{district,i}^{dhn} = Q_{aggregated,i}^{dhn} - Q_{loss,i}^{dhn} \quad (5.16)$$

Network Heat Losses

The heat losses of the district heating network to the ground are calculated using a method developed P. Wallentén [6]. The method calculates the steady-state heat losses of two buried insulated pipes, each containing water at a different temperature. Figure 5.1 illustrates the setup and introduces the variables described in Table 5.7. Here, the pipe depth H and the half-distance between them D are assumed to be 1 m and 0.5 m, respectively. The thermal conductivity of the ground is considered to be 2.1 W/(m · K) [7].

The energy flow model requires the steady-state heat losses of the two pipes combined. Assuming a constant temperature and radius along the pipe's length, the specific steady-state heat losses of the two pipes combined are defined as [6]:

$$q_1 + q_2 = 2 \cdot q_s = 4 \cdot \pi \cdot \lambda_g \cdot (T_s - T_0) \cdot h_s \quad (5.17)$$

where T_s [°C] denotes the average temperature of the water in the pipes. The dimensionless heat loss factor h_s is defined by:

$$h_s^{-1} = \ln\left(\frac{2H}{r_0}\right) + \frac{\lambda_g}{\lambda_i} \cdot \ln\left(\frac{r_0}{r_i}\right) + \ln\left(1 + \sqrt{1 + \left(\frac{H}{D}\right)^2}\right) \quad (5.18)$$
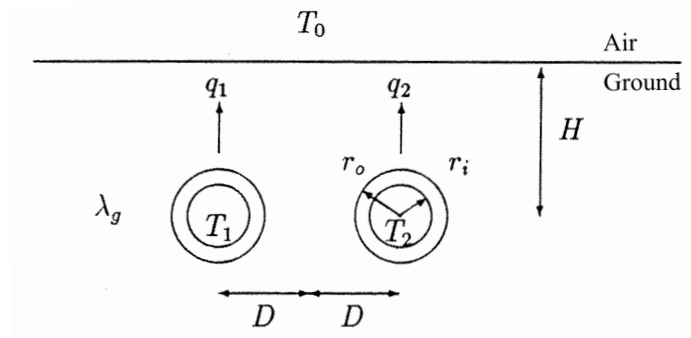
FIGURE 5.1: Supply and return pipes of district heating network, adapted from [6]

H	Depth of the pipes	[m]
D	Half the distance between the pipes	[m]
r_o	Outer radius of the pipe	[m]
r_i	Inner radius of the pipe	[m]
λ_i	Ground thermal conductivity	[W/(m $\cdot$ K)]
λ_o	Insulation thermal conductivity	[W/(m $\cdot$ K)]
T_0	Temperature of the ground surface	[°C]
T_1	Water temperature in pipe 1	[°C]
T_2	Water temperature in pipe 2	[°C]
q_1	Specific heat loss from pipe 1	[W/m^2]
q_2	Specific heat loss from pipe 2	[W/m^2]

TABLE 5.7: Overview of district heating network heat loss variables, adapted from [14]

The hourly steady-state heat loss $Q_{loss,i}^{dhn}$ [Wh] for the entire network, considering L [m] the length of the hot pipe plus the cold pipe, denotes:

$$Q_{loss,i}^{dhn} = 4 \cdot \pi \cdot \lambda_g \cdot \left(T_{avg,i}^{dhn} - T_{ground} \right) \cdot h_s \cdot L \tag{5.19}$$

where T_{ground} [°C] is the constant temperature of the surrounding ground, assumed to be 10°C. The average network temperature, $T_{avg,i}^{dhn}$[°C], is calculated as the mean of the temperature of the cold pipe, $T_{cold,i}^{dhn}$, and the hot pipe, $T_{hot,i}^{dhn}$.

5.5.2 Component Parameters

The parameters used for modeling the behavior of the district heating network are obtained from the Logstor product catalog [15]. From this catalog, the PexFlextra pipes are selected. These pipes are available in two degrees of insulation thickness and with different inner diameters. Due to the higher water temperatures in the fourth-generation systems (4Ga and 4Gb), highly insulated pipes are allocated to these systems. The fifth-generation systems that operate at lower temperatures

utilize pipes with reduced insulation. The inner diameter is estimated based on the district's aggregated load profile $Q_{district,i}^{dhn}$ [wh]. The network inner radius r_i [m] is determined by the district peak load $\dot{Q}_{district,max}^{dhn}$ [w], ensuring that the maximum water velocity does not exceed a specified limit:

$$\dot{Q}_{district,max}^{dhn} = \pi \cdot r_i^2 \cdot v_{w,max} \cdot \rho_w \cdot c_{p,w} \cdot \Delta T_{pipes}^{dhn} \tag{5.20}$$

Here, the maximum allowable water velocity, $v_{w,max}$ for the considered PexFlextra pipes is 2.5 m/s [15]. The temperature difference between the hot and cold pipes, ΔT_{pipes}^{dhn} [°C], depends on the operating mode of the district heating network, detailed in Section 5.7. Table 5.8 summarizes the relevant pipe parameter values.

Logstor PexFlextra	
High insulation thickness [m]	0.085
Low insulation thickness [m]	0.065
Insulation thermal conductivity [W/(m · K)]	0.022

Table 5.8: Technical data of district heating network pipes [15]

The investment cost of the district heating network is estimated based on the total length of the network. For a district containing 50 buildings, a total pipe length L of 1600 m is considered. The specific investment cost per meter is 250 €/m for low-insulated pipes and 400 €/m for high-insulated pipes [10], as shown in Table A.1.

5.6 Buffer Tank

All systems contain a buffer tank situated between the district and the central heat pump or heat exchanger connected to the borefield storage. The main goal of the buffer tank is to reduce the peak load on the centralized components and lower their investment cost.

5.6.1 General Equations

The capacity of the buffer tank, Q_{buffer} [Wh], is determined such the buffer tank can average out the peak load of the district load profile, $Q_{district,i}^{dhn}$, over an 8-hour period. The tank is modelled as a perfectly stratified tank with a hot and a cold volume. The total tank volume, V_{buffer} [m^3], can be calculated using the following equation:

$$Q_{buffer} = \rho_w \cdot c_{p,w} \cdot V_{buffer} \cdot \Delta T_{pipes}^{dhn} \tag{5.21}$$

The temperature difference between the hot and cold volumes in the buffer tank is assumed to be equal to the difference between the hot and the cold pipe of the network, ΔT_{pipes}^{dhn} [°C]. The pipe temperature depends on the operation of the district heating network, which is explained in Section 5.7. Finally, the buffer tank's losses are neglected compared to the district's overall aggregated heat load due to the relatively small size of the tank.

5.6.2 Component Parameters

Once the volume of the buffer tank is defined, the next step is to calculate the investment cost associated with the tank. For this, the cost correlation for thermal storage tanks ranging from 0.5 m^3 to 500 m^3 is used from the study by Mauther et al. [23]. This correlation has been derived from real-life project data, providing a reliable estimate for investment costs. The investment cost IC_{buffer} [€] in terms of the tank volume V_{buffer} [m^3] is expressed as follows:

$$IC_{buffer} = 750 \cdot V_{buffer} + 403.5 \cdot (V_{buffer})^{0.5324} \qquad (5.22)$$

The cost consists of a linear term scaling directly with the volume added with a sublinear term. Therefore, larger tanks are more cost-effective on a per-unit basis. This cost function is also presented in Table A.1.

5.7 Central Heat Pump and Central Heat Exchanger

The central heat pump and heat exchanger are crucial in transferring the thermal load from the buffer tank to the borefield. In 4th-generation networks, the central heat pump is used for providing heating and active cooling, while the central heat exchanger is used for passive cooling. In 5th-generation networks, only a heat exchanger is installed centrally to directly transfer heat and cold.

5.7.1 General Equations

Out of the central heat pump and the central heat exchanger, only the central heat pump is modeled. However, they both influence the district heating network water temperatures. The first section elaborates on these temperatures and the second section delivers the equations of the central heat pump.

District heating Network Temperatures

The operational temperatures within the district heating network are determined by which central component is activated, as outlined in Table 5.6. In 4th-generation systems, the central heat pump is activated when the buffer tank load indicates a heating requirement (negative load profile). The heat pump extracts energy from the borefield and raises the temperature of the network's hot pipe, $T_{hot,i}^{dhn}$ [°C] to 37°C. This temperature ensures the necessary supply temperature of 35°C for space heating, with an additional 2°C to account for the heat exchanger between the network and the dwellings. A standard 5°C temperature difference is maintained over the borefield and between the network pipes, resulting in a cold pipe temperature $T_{cold,i}^{dhn}$ [°C] of 32°C [40]. In scenarios where passive cooling is insufficient to meet cooling demands (i.e. when it cannot deliver a cooling temperature of 18°C at the dwelling), the heat pump is engaged for active cooling. In such cases, the cold pipe temperature is maintained at 16°C, again considering a 2°C differential across the residential heat exchanger. The central heat exchanger is utilized for passive cooling

39

in 4th-generation systems and for heating and cooling in 5th-generation systems. This component facilitates thermal exchange with the borefield, maintaining a consistent 3°C temperature differential across the network pipes and between the borefield's inlet and outlet [40]. Assuming a negligible temperature drop over the central heat exchanger, the network temperatures at any given hour i are calculated by adding and subtracting 1.5°C from the average borefield fluid temperature $T_{borefield,i}^{fluid}$ [°C].

	HP Heating	HP Cooling	Central Heat Exchanger
$T_{hot,i}^{dhn}$	37°C	19°C	$T_{borefield,i}^{fluid} + 1.5°C$
$T_{cold,i}^{dhn}$	32°C	16°C	$T_{borefield,i}^{fluid} - 1.5°C$

TABLE 5.9: Network temperatures $T_{hot,i}^{dhn}$ [°C] and $T_{cold,i}^{dhn}$ [°C] for activated central heat pump (HP) and for activated central heat exchanger, with borefield fluid temperature $T_{borefield,i}^{fluid}$ [°C].

Central Heat Pump Equations

The hourly heating and cooling load the heat pump generates to meet the buffer tank's demand are denoted as $Q_{central,i}^{h}$ [Wh] and $Q_{central,i}^{c}$ [Wh], respectively. These loads are directly linked to the corresponding electricity consumption, $W_{central,i}^{h}$ [Wh] for heating and $W_{central,i}^{c}$ [Wh] for cooling, through the coefficient of performance for heating, COP_{i}^{h}, and cooling, COP_{R}^{c}:

$$Q_{central,i}^{h} = COP_{i}^{h} \cdot W_{central,i}^{h} \qquad (5.23)$$

$$Q_{central,i}^{c} = COP_{R}^{c} \cdot W_{central,i}^{c} \quad \text{for } T_{central,i}^{sink,c} > 16°C \qquad (5.24)$$

where the heat sink temperature $T_{central,i}^{sink,c}$ [°C] is equal to average borefield fluid temperature, $T_{borefield,i}^{fluid}$ [°C], minus 2.5°C. This adjustment accounts for the temperature 5°C temperature difference across the borefield. In the equation, the heating performance coefficient COP_{i}^{h} is calculated by the linear relationship with its source temperature $T_{central,i}^{source,h}$ [°C]:

$$COP_{i}^{h} = a_{central}^{h} \cdot T_{central,i}^{source,h} + b_{central}^{h} \qquad (5.25)$$

The source temperature for the central heat pump is defined as the average borefield fluid temperature, $T_{borefield,i}^{fluid}$ [°C], increased by 2.5°C.

5.7.2 Component Parameters

The heat pump-specific parameters for generating heat at 37°C are given in Table 5.10. These parameters are derived from a linear interpolation of data from the Vitocal 300-G Pro datasheet [52]. This particular heat pump model, produced by Viessmann, is a ground-source system designed for large-scale applications such as district heating. The refrigeration coefficient of performance COP_{R}^{c} is considered a constant value of 5.8. To determine the load profile of the heat pump on the borefield,

equations are applied analog to Equations (5.13) and (5.14) which define the heat load of the residential heat pump on the network.

Central Heat Pump	
$a_{central}^h$	0.069
$b_{central}^h$	3.847

TABLE 5.10: Linear interpolated COP curve coefficients of the Vitocal 300-G Pro ground source heat pump [12]

The sizing and investment cost of the central heat pump are determined based on the peak demand of the buffer tank load profile. The cost function, as a linear relationship of the buffer tank peak load in Wh, is outlined in Table A.1. On the other hand, the central heat exchanger is, being relatively inexpensive, has its costs neglected.

5.8 Borefield

The borefield serves as the seasonal thermal storage unit across all systems, which is essential for managing heat demand and supply within the district. It stores excess thermal energy and delivers it when needed to meet district heating and cooling demands. The central heat pump or central heat exchanger facilitates this process by either extracting or injecting heat into the borefield. The thermal balance within the borefield is crucial; if more heat is extracted than injected over time, the borefield temperature will decrease, and vice versa. Therefore, proper sizing of the borefield is essential to ensure that its temperature remains within predefined operational limits over its lifetime. This section outlines the methodology for sizing the borefield and provides the numerical values used in the model.

5.8.1 General Equations and Sizing Methodology

The borefield is sized using a double iterative method, as described by Coninx et al. [7]. This method utilizes the L4 sizing method of the GHEtool, an open-source Python package developed by Peere et al. [53]. The GHEtool calculates the necessary borefield size, specifically its total length, based on an hourly load profile. The tool models the borehole temperature response, $T_{borefield,i}^{hole}$ [°C], to this load profile using g-functions. These g-functions characterize the ground's thermal response to a given thermal load pulse, depending on the borefield layout. For a given hourly load profile, which consists of a series of thermal pulses, the resulting thermal responses are superimposed to determine the hourly borehole temperature profile. This borehole temperature relates to the average borefield fluid temperature $T_{borefield,i}^{fluid}$ [°C] and the equivalent thermal borehole resistance R_b^* [m·K /W] as follows:

$$T_{borefield,i}^{fluid} = T_{borefield,i}^{hole} + \frac{\dot{Q}_{borefield,i} \cdot R_b^*}{n_{hole} \cdot L_{hole}} \tag{5.26}$$
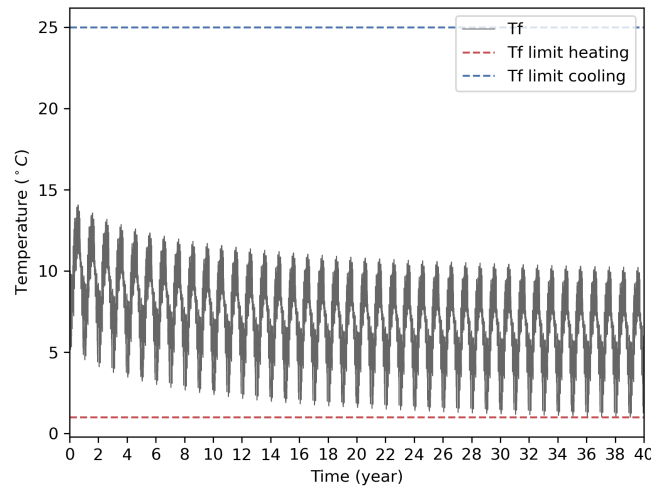
FIGURE 5.2: Example of the borefield fluid temperature T_f evolution and its limits.

with $\dot{Q}_{borefield,i}$ [W] the power of the thermal load on the borefield, and n_{hole} the number of holes with depth L_{hole} [m]. This equation demonstrates that to maintain a constant fluid temperature range, reducing the depth (and thus the overall size) of the borefield requires an increase in the temperature differential between the fluid and the borehole. However, the fluid temperature must always stay within a limited range. The most cost-efficient design is achieved by finding the smallest borefield that can maintain the fluid temperature within its limits. The GHEtool accomplishes this through an iterative process, determining the optimal borehole depth and the corresponding average fluid temperature profile.

Figure 5.2 shows an example borefield fluid temperature profile that stays within its boundaries during the lifetime of an optimally sized borefield. Initially, the fluid temperature starts at the undisturbed ground temperature, typically around 10°C. Over time, the profile shows seasonal variations, with peaks corresponding to heat injection and extraction periods. In this scenario, heating demands are predominant, leading to a gradual decrease in the average borefield temperature over the years. The fluid temperature eventually reaches its lower limit during a peak heating demand in the final year of the borefield's lifetime.

Up to this point, the borefield size and fluid temperature profile have been determined based on a predefined district load profile. However, it's important to note that the district load itself is influenced by the borefield fluid temperature. This temperature impacts the performance of temperature-dependent components like heat pump coefficients of performance and the efficiency of solar thermal collectors. Therefore, to accurately determine both the district load and borefield size, a second iterative loop is introduced, which allows for simultaneous optimization of these parameters. Figure 5.3 illustrates the schematic representation of the iterative
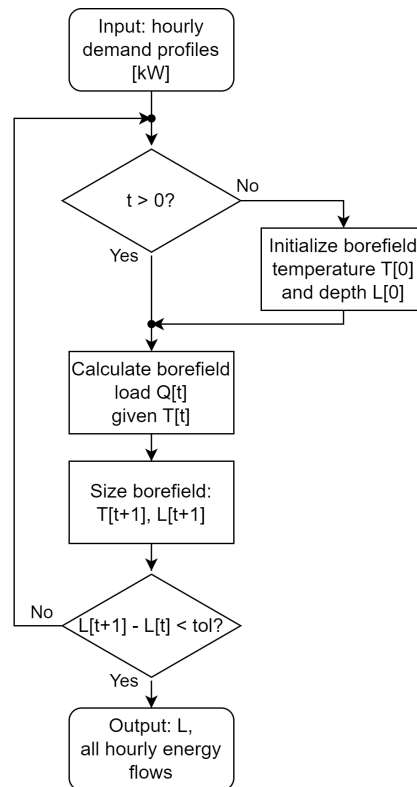
FIGURE 5.3: Schematic representation of iterative borefield sizing algorithm based on [7] (T: borefield temperature, L: borefield depth, and Q: borefield load)

borefield sizing algorithm for each iteration t. Starting at t equals zero, an initial borefield fluid temperature profile and depth are assumed. Using the temperature profile and the input demand profiles, the load on the borefield is computed utilizing the component models of all thermal components. Then, an iterative optimal borefield sizing is done using GHE-tool, determining a new fluid temperature profile and depth. The new temperature profile is used in the next outer loop iteration until the borefield depth converges within a tolerance of 0.1m. Once convergence is achieved, the final borefield size and all corresponding thermal energy flows are established. These calculated energy flows are then used to size the other thermal components within the system, thereby fully defining the thermal part of the system.

5.8.2 Component Parameters

The model uses specific numerical values for the borefield and ground parameters, as listed in Table 5.11. The borefield is configured as a square grid with 8 by 8 boreholes spaced 6 meters apart. The lower limit of the average borefield fluid temperature is set at 1°C to prevent freezing, and the upper limit is 25°C to maintain the groundwater quality [54]. The investment cost for the borefield is calculated based on the total borehole length, with an assumed cost of 35 €/m according to [7],

as detailed in Table A.1

Borefield parameters	
Configuration boreholes	8 x 8 holes
Borehole spacing x-direction [m]	6
Borehole spacing y-direction [m]	6
Borehole diameter [m]	0.075
Equivalent Borehole resistance $[\text{W}/(\text{m} \cdot \text{K})]$	0.12
Maximum average fluid temperature $[°\text{C}]$	25
Minimum average fluid temperature $[°\text{C}]$	1
Ground parameters	
Undisturbed ground temperature $[°\text{C}]$	11
Ground thermal conductivity $[\text{W}/(\text{m} \cdot \text{K})]$	2.1

TABLE 5.11: Overview of the borefield and ground parameters [7, 10]

5.9 Grid Connected PV Home-Battery System

Each dwelling of the four selected energy systems has a grid-connected PV installation with a home battery. This setup allows a part of the residential electric demand to be met by solar-generated and stored electricity while the remainder is supplied by the grid.

5.9.1 General Equations

Since all the heat and electricity flows of the thermal components are defined in previous sections, the total electric demand of one dwelling, $W_{dwelling,i}$ [Wh], can be written as follows:

$$W_{dwelling,i} = W_{demand,i} + W_{hp,i}^{dhw} + W_{hp,i}^{sh} + W_{hp,i}^{sc} \tag{5.27}$$

$$\tag{5.28}$$

In this equation, the electric contributions of the building heat pumps are added to the electric household demand, $W_{demand,i}$ [Wh]. When a heat pump is not installed in the system, its corresponding term becomes zero. The electric demand for household appliances for each hour i is known by the given demand profile. To determine the hourly electric load of the dwelling on the grid, $W_{dwelling,i}^{grid}$ [Wh], the contribution of the PV panels and the battery should be combined with the dwelling load as follows:

$$W_{dwelling,i}^{grid} = \eta_{converter} \cdot (W_{pv,i} - \eta_{battery} \cdot \Delta C_{battery,i}) - W_{dwelling,i} \tag{5.29}$$

Here, $W_{pv,i}$ [Wh] corresponds to the generated PV electricity, and $\Delta C_{battery,i}$ [Wh] is the electricity used to charge the battery. Note that the value of $\Delta C_{battery,i}$ is

negative when the battery electricity is discharged. In the equation, efficiencies $\eta_{converter}$ and $\eta_{battery}$ respectively account for the electricity passing the converter or being charged and discharged.

The equations for the PV electricity generation of n_{pv} panels and their efficiency $\eta_{pv,i}$ from introductory Section 2.1 are repeated and adapted to each hour i:

$$W_{pv,i} = n_{pv} \cdot \eta_{pv,i} \cdot A_{pv} \cdot G_i \tag{5.30}$$

$$\eta_{pv,i} = \eta_{pv,rated}\left(1 - \gamma \cdot (T_{cell,i} - NOCT)\right) \tag{5.31}$$

With A_{pv} [m^3] the panel surface, $\eta_{pv,rated}$ the rated efficiency, $NOCT$ [°C] the Nominal Operating Cell Temperature, and γ [°C^{-1}] the temperature coefficient, being characteristics of the selected PV panel. Finally, the panel irradiation, G_i [W/m^2], and the PV cell temperature, $T_{cell,i}$ [°C], for each hour i are known from given hourly profiles in Section 4.3.

It is important to mention that the electric power of the central heat pump for heating, $W_{central,i}^h$ [Wh], and cooling, $W_{central,i}^c$ [Wh], are not included in the single dwelling demand. This electric load, $W_{central,i}^{grid}$ [Wh], is provided by a separate grid connection located at the central heat pump, without the intervention of PV panels nor batteries:

$$W_{central,i}^{grid} = -W_{central,i}^h - W_{central,i}^c \tag{5.32}$$

5.9.2 Component Parameters

The model performs energy calculations on a system with a predefined number of PV panels and solar thermal collectors installed on the dwellings. Therefore, the number of PV panels of a residential PV installation and its cost is known, using a fixed cost per panel given in Table A.1 [20]. The specifications, including efficiency parameters and peak power for the PV panels, are derived from the Trinasolar Vertex S TSM-415 datasheet [16]. The efficiency parameters of the Pv panel and its peak power are shown in Table 5.12. Notably, the model considers a PV panel area equal to the solar thermal collector area to make a fair trade-off, given a limited roof area.

The hybrid converter is characterized using data from the Huawei SUN2000 KTL-L1 [17] of which the parameters are also given by Table 5.12. The converter size is based on the total peak power of the PV installation (kWp), with a reduction ratio of 2/3, as indicated in the datasheet. The investment cost for the inverter is calculated using a linear cost curve, depending on the inverter's power rating, as shown in Table A.1.

The battery capacity in Wh increases with the size of the PV installation but is capped based on the dwelling's electricity demand profile. This limitation ensures that the storage capacity does not exceed the amount of stored PV electricity that can be discharged. The battery size is determined by the minimum difference between the average daily excess PV generation and the average daily grid demand of the

dwelling, both calculated without a battery. Then, the energy flows are recalculated once the appropriately sized battery is installed.

Additionally, the feasibility of installing a battery is assessed using the total cost equations from Section 4.2.1. The battery is removed if the operational benefit does not justify the investment and annual maintenance costs. The operational benefits are calculated as the product of the electricity discharged and the price difference between grid offtake and injection.

For the residential battery, the model uses a Lithium-ion battery, such as the Huawei LUNA2000, with an assumed round-trip efficiency of 90%, a typical value for this type of battery [18]. The battery's cost is also determined by a linear function based on its capacity, as presented in Table A.1.

PV Panel	
Area A_{pv} [m^2]	1.99
Rated efficiency $\eta_{pv,rated}$	0.208
Temperature coefficient γ [°C^{-1}]	-0.0034
Nominal operating cell temperature $NOCT$ [°C]	45
Peak power [kWp]	0.415
Hybrid Converter	
Efficiency $\eta_{converter}$	0.95
kW/kWp ratio	2/3
Home Battery	
Efficiency $\eta_{battery}$	0.9

TABLE 5.12: Technical data of the PV panel, hybrid converter, and home battery [16, 17, 18]

Chapter 6

Results and Discussion

In this chapter, the results of the energy-flow calculations are discussed. First, the performance of different configurations of PV and STC panels in terms of the Total Cost of Ownership (TCO) and annual CO_2 emissions are assessed separately in Sections 6.1 and 6.2 for all four systems. These two performance indicators are calculated for various rooftop PV/STC configurations, considering a dwelling's roof capacity of 12 panels. This analysis reveals trends that depend on the configuration. Following this, Section 6.3 compares the performance across both metrics of all four systems, focusing on relevant configurations, particularly, those where the roof is fully covered. In Section 6.4, a sensitivity analysis is conducted to evaluate the impact of varying specific parameters on TCO and CO_2 emissions. Finally, the key takeaways from these sections are synthesized into a set of guidelines in Section 6.5, offering recommendations on the use of solar PV panels and STCs in residential districts with a collective seasonal borehole thermal energy storage.

6.1 Total Cost of Ownership Assessment

In all considered cases, the calculations reveal that the home battery is unprofitable in the modeled systems. Therefore, the analysis in this section, as well as in Sections 6.2 and 6.3 is conducted with the battery removed from the systems. However, Section 6.4 which includes a sensitivity analysis of electricity tariffs, discusses scenarios where the battery becomes feasible.

Figure 6.1 presents plots of the TCO for all four systems across all combinations of PV panels and STCs on the roof of each dwelling, assuming a roof capacity of 12 panels. A maximum of five STCs is considered, as adding more collectors significantly increases costs across all systems. A system with a lower total cost is more optimal since it meets the energy demand at a reduced cost. When starting from the base case (0 PV and 0 STC) and adding PV panels or STCs, some clear trends emerge.

First, in all systems, adding PV panels reduces the TCO compared to the base case because the electricity cost savings from the PV installation outweigh its investment

cost. However, the marginal benefit —the benefit of adding one unit— of adding additional PV panels decreases as more panels are installed. This occurs because a larger PV installation, without a battery, saturates the instantaneous electricity demand more quickly, leading to more excess electricity being injected into the grid. The feed-in remuneration received for this injected electricity is significantly lower than the offtake tariff, lowering the monetary gains of additional PV panels

Next, in all four systems, an excessive number of STCs causes the TCO to increase substantially. This is because adding collectors and thereby increasing annual borefield regeneration raises the borefield temperature. As explained in Section 5.8.1, there is a maximum allowed borefield temperature considered in the borefield sizing method. In cases of excessive regeneration, the borefield is sized larger to store more heat without exceeding the temperature limit. This increased borefield size, combined with the addition of expensive STCs, results in significant cost increases.

Finally, the cost-optimal configuration for the a-systems is full PV (12PV/0STC), while in the b-systems, two PV panels are replaced by STCs (10PV/2STC). To understand this behavior, detailed reasoning for the individual systems is provided in the following sections. Note that systems 4Ga and 5Ga show similar TCO surface shapes with an offset in TCO, as do the systems 4Gb and 5Gb. Therefore, detailed discussions are provided only for the 4Ga and 4Gb TCO graphs in Sections 6.1.1 and 6.1.2, which contain insights applicable to systems 5Ga and 5Gb. The cost offset between the 4th and 5th generation systems is discussed in Section 6.1.4.

6.1.1 Total Cost of Ownership of System 4Ga

The TCO of System 4Ga can be broken down into the Investment Cost (IC) and the Operational Cost (OC). To enhance clarity, the graphs of the system's TCO, IC, and OC are sliced along a constant number of PV panels and projected onto a 2D plane, as shown in Figure 6.2. Each colored curve represents configurations with the same number of PV panels but varying numbers of STCs. Significant cost savings are achieved by moving from the base case configuration (0PV/0STC) to the configuration with 12 PV panels and 0 STC. In fact, full PV is the optimal configuration for this system in terms of total cost, as the OC improvements gained from adding STCs do not offset the increased IC. Nonetheless, several trends appear when STCs are included in the system.

Starting from the base case configuration in Figure 6.2a, adding one STC has little effect on the system's TCO because the increase in IC is compensated by the decrease in OC. However, when starting from a configuration that already includes many PV panels (e.g., 10PV/0STC), adding one STC leads to a noticeable increase in TCO. This difference in TCO is solely due to OC variation, as the IC curves for different numbers of PV panels run parallel. To understand this OC variation, it is important to note that the primary use of STC heat is to charge the DHW tank, saving electricity

(A) Total Cost 4Ga

(B) Total Cost 4Gb

(C) Total Cost 5Ga
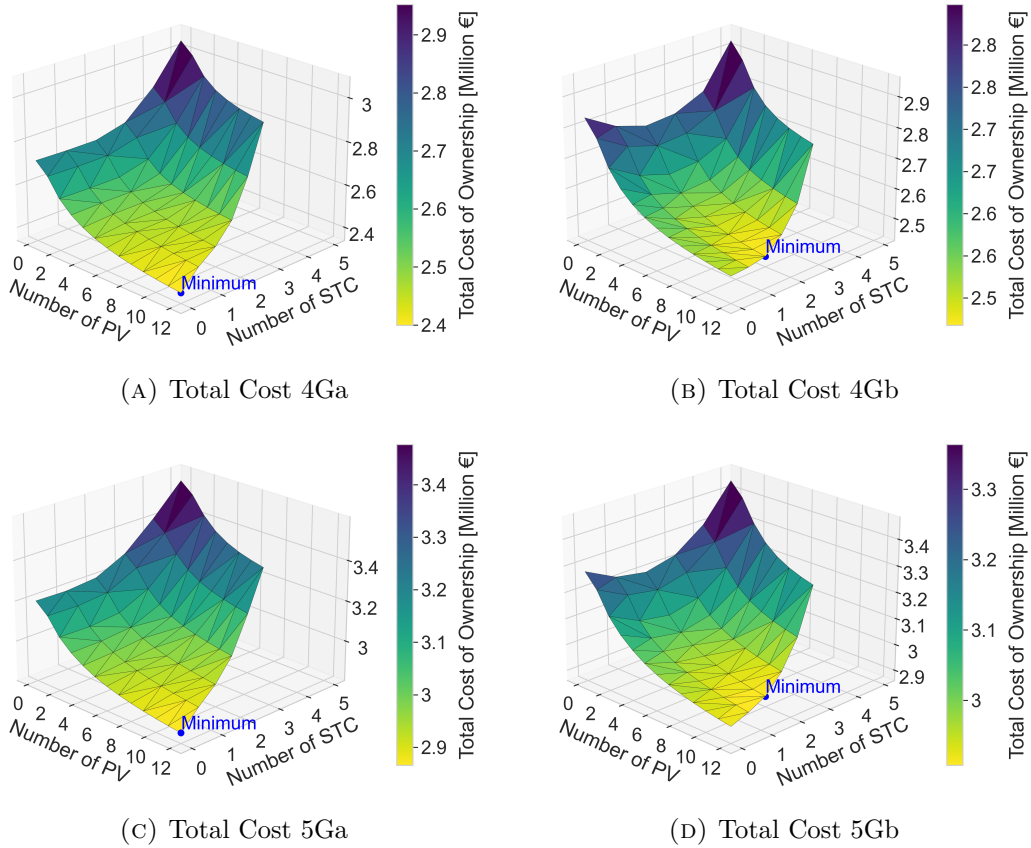
(D) Total Cost 5Gb

FIGURE 6.1: Total Cost of Ownership for different PV/STC configurations for all four systems

costs for the DHW heat pump. Since a PV installation reduces electricity costs by generating electricity for direct use and grid injection, the electricity cost savings for the DHW heat pump from the first added STC are diminished when more PV is installed. Additionally, reducing the dwelling's electricity demand by mitigating DHW heat pump use decreases the self-utilization of PV electricity, resulting in more grid injection at lower tariffs. In conclusion, when PV panels and STCs are both used for DHW, they harm each other's operational benefits. This effect lessens as more collectors are added, as the relative share of generated DHW heat compared to borefield regeneration decreases with the saturation of DHW demand.

Adding a second STC affects the OC curves in Figure 6.2b due to the saturation of the DHW load, leading to more heat being redirected to the borefield for regeneration. This borefield cost reduction results in a less steep IC curve around the addition of two STCs in Figure 6.2b. However, adding more than 3 STCs causes the IC curve to rise sharply because the borefield must be sized larger to handle excess regeneration while keeping the borefield temperature within its limits. The altered borefield

temperature also necessitates active cooling with a heat pump instead of passive cooling with a heat exchanger. This increase in active cooling demand raises the OC curve when more than 2 STCs are installed. Finally, it can be observed that the OC curves are slightly concave in the region of three to five STCs. This flattening is due to electricity savings from higher heat pump coefficients of performance resulting from increased borefield temperatures during space heating.

(A) Total Cost 4Ga

(B) Operational Cost 4Ga

(C) Investment Cost 4Ga

FIGURE 6.2: 2D projection of Total Cost of Ownership, Operational Cost, and Investment Cost graphs for different PV/STC configurations in System 4Ga

6.1.2 Total Cost of Ownership of System 4Gb

Figure 6.3 shows the projected slices of the TCO graphs and its components for System 4Gb. Just like system 4Ga, significant TCO savings are realized when moving from the base case configurations to full PV. In this system, additional cost savings can be achieved by swapping 2 PV panels for STCs to reach the cost-optimal configuration. System 4Gb has a larger borefield heat demand compared to 4Ga because it extracts heat for both domestic hot water (DHW) and space heating. Consequently, 4Gb features a larger and more expensive borefield in the base case, leading to greater cost savings when regenerated. In the model, including 2 STCs in

4Gb results in a borefield depth reduction of 50 m, whereas 4Ga only reduces the depth by a smaller amount. This is reflected in the IC curves remaining relatively stable when the first 2 STCs are added, indicating that the additional investment cost of replacing PV panels with the more expensive STCs is largely offset by the borefield cost reduction. As observed in System 4Ga, the operational OC curve of 4Gb also exhibits the reduced benefits of the first added STCs due to installed PV, the active cooling effect, and the increased COP from additional STCs. However, the increased COP effect is not visible in the OC curve of 4Gb because the borefield temperatures do not reach sufficiently high levels with the regeneration of 5 STCs, due to the higher borefield heat demand.

(A) Total Cost System 4Gb

(B) Operational Cost 4Gb
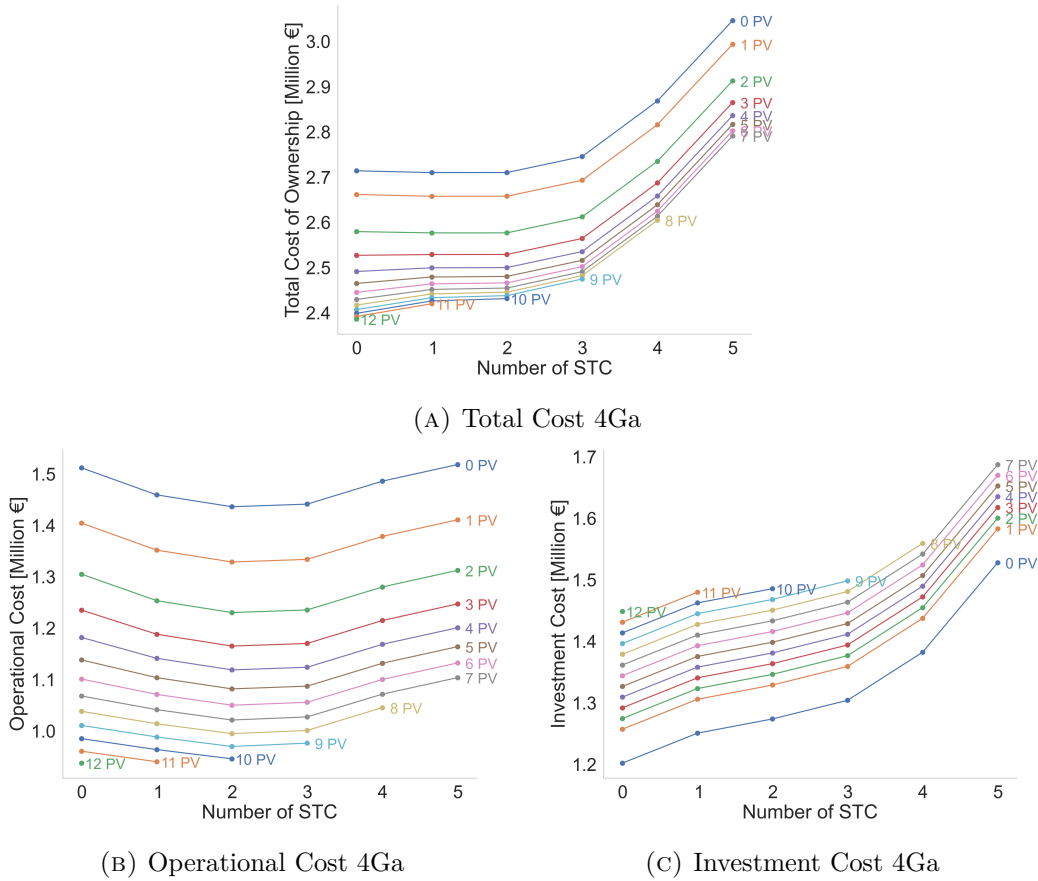

(C) Investment Cost 4Gb
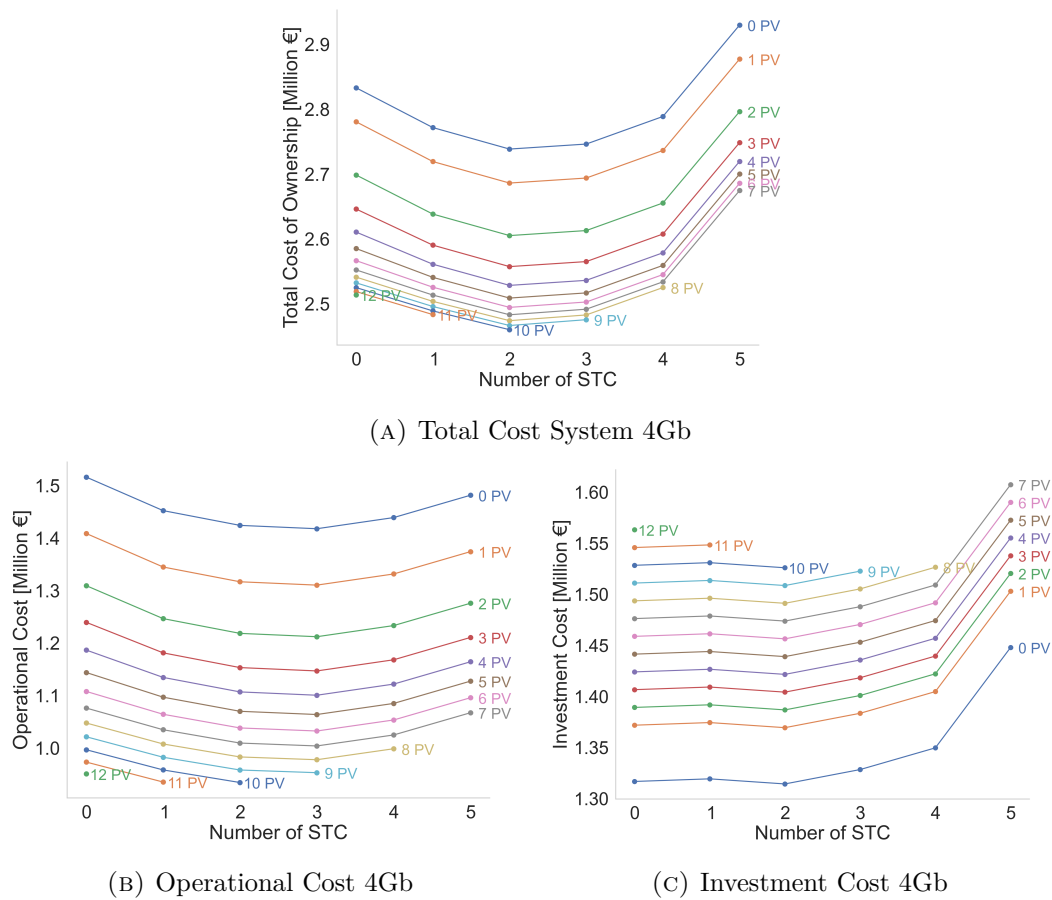
FIGURE 6.3: 2D projection of Total Cost of Ownership, Operational Cost, and Investment Cost graphs for different PV/STC configurations in system 4Gb

6.1.3 Total Cost of Ownership of Systems 5a and 5b

The sliced Total Cost graphs of systems 5Ga and 5Gb, presented in Figure 6.4, show trends similar to those observed for systems 4Ga and 4Gb. The same reasoning about the reduced DHW benefit of the first STC when PV is installed, borefield cost reduction, active cooling effects, and increased COP can be developed again.
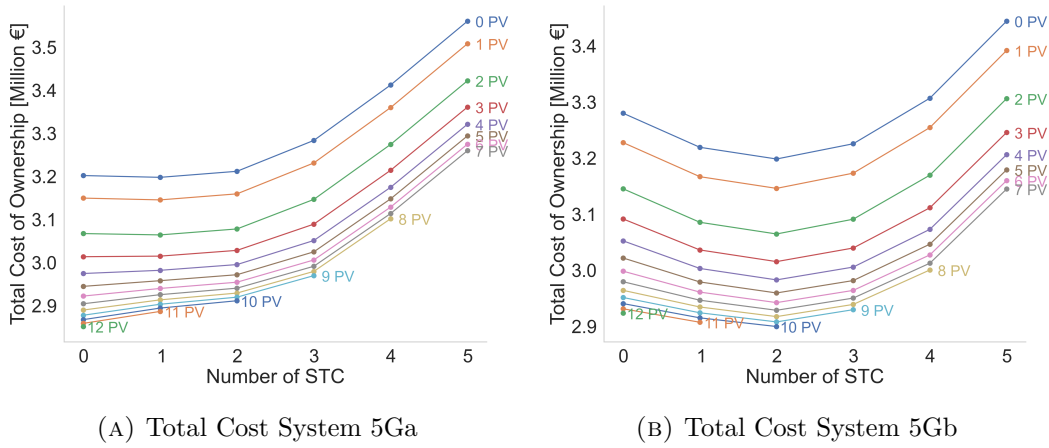
51

(A) Total Cost System 5Ga

(B) Total Cost System 5Gb

FIGURE 6.4: 2D projections of the Total Cost of Ownership graphs for different PV/STC configurations in systems 5Ga and 5Gb

6.1.4 Total Cost of Ownership Contributions

To investigate the TCO offset between the 4G and 5G district heating systems, the TCO contributions of all systems, each equipped with 10 PV panels and 2 STCs, are shown in Figure 6.5. The bar chart clearly indicates that the investment costs account for the majority of the difference between the 4G and 5G systems. While the 4G network costs are higher due to the modified insulation level, the residential water-to-water heat pump (HP) costs of the 5G systems dominate compared to the costs of the central and residential DHW heat pumps of the 4G systems. Additionally, the borefield costs of the b-systems are higher than those of the a-systems due to the increased DHW heat demand on the borefield. The borefield costs of the 4G systems are higher compared to their 5G counterparts because the 5G systems operate at a lower district heating network temperature. This results in enhanced borefield regeneration due to increased STC efficiency. Figure 6.6 illustrates how STCs contribute to greater borefield regeneration in 5G systems. It is also evident that borefield regeneration is significantly influenced by a low STC fluid flow rate and excess heat gain when the DHW tank is fully charged. Notably, STCs can generate more heat energy per unit surface area compared to PV panels generating electrical energy because STCs typically have higher efficiency.

Regarding the difference in OC, the maintenance costs of the 5G systems are higher, as they are a fraction of the initial investment cost which is larger for 5G systems compared to 4G systems. The electricity cost and demand over the project lifetime are broken down into their components and plotted in Figure 6.7 for all four systems with the 10 PV/2 STC configuration. The electricity grid cost and demand for the 5G systems are slightly lower, primarily because 5G systems enable greater self-utilization of the PV-generated electricity. This occurs because the central heat pump in the 4G systems is not directly powered by the residential PV panels, leading to a higher amount of electricity being sold back to the grid.
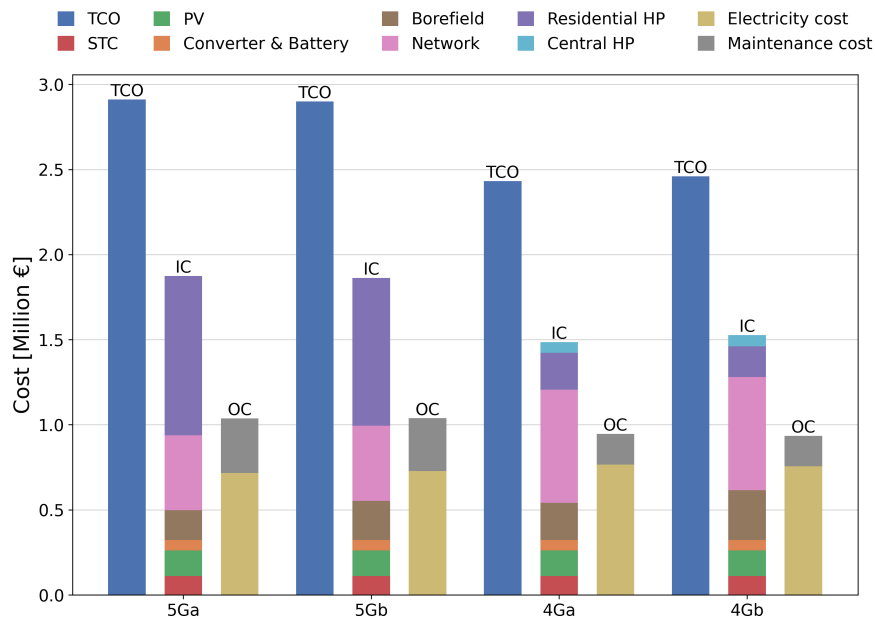
FIGURE 6.5: Total Cost of Ownership contributions of all four systems in configuration 10PV/2STC
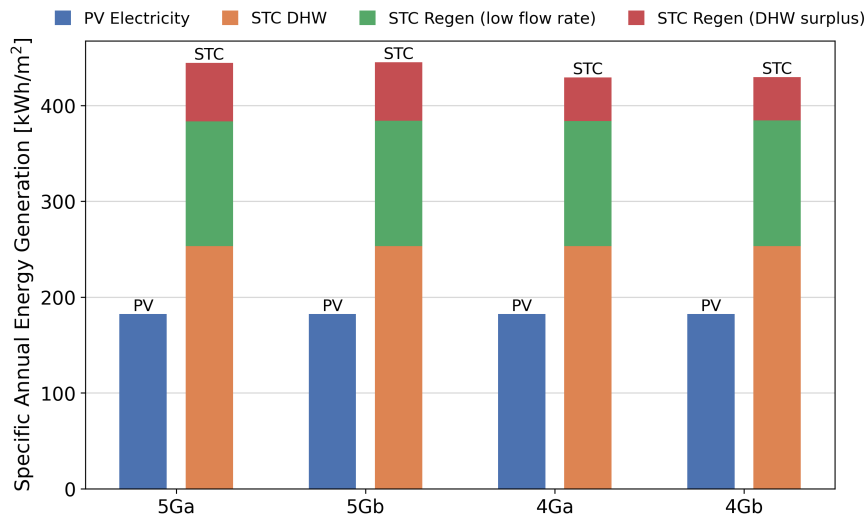

FIGURE 6.6: Specific annual generated energy of PV and STC in all four systems with configuration 10PV/2STC
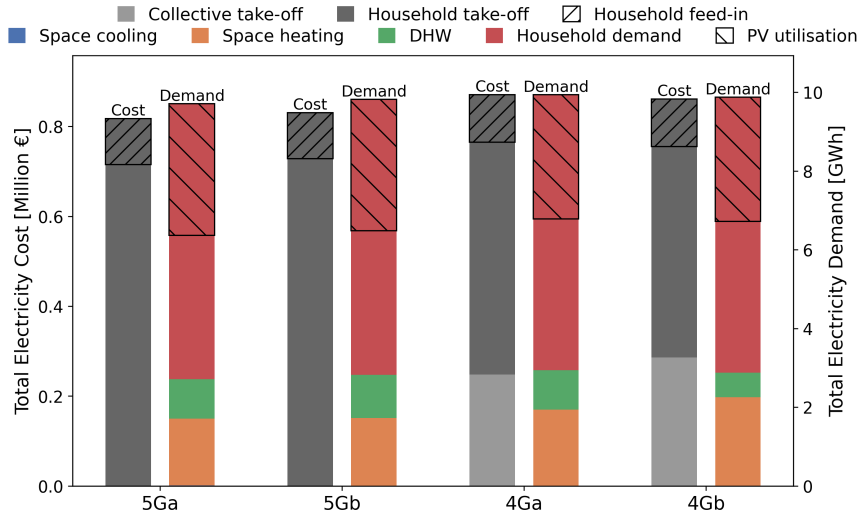
FIGURE 6.7: Electricity cost and demand contributions of all four systems in configuration 10PV/2STC

In conclusion, in 5G systems, PV panels reduce electricity costs and grid demand more effectively, and STCs contribute to more borefield regeneration compared to 4G systems. However, the substantial investment cost of residential water-water heat pumps overshadows these benefits of 5G systems, making 5G systems more expensive overall. Thus, the cost offset between the systems is primarily caused by the selected system components rather than the performance of the PV panels and STCs.

6.2 Annual CO$_2$ Emissions Assessment

The graphs in Figure 6.8 represent the annual CO$_2$ emissions for different configurations across the four systems. Since these systems do not use fossil fuels, the only source of operational emissions is the energy drawn from the electric grid, which has a specific CO$_2$ content per kWh. Opting for a full PV configuration leads to significant emission reductions in all four systems compared to the base case, as PV panels reduce grid utilization by directly supplying the electric demand. These reductions are more pronounced in the 5G systems because, in 4G systems, the PV panels do not decrease the grid electricity demand for the central heat pump. Additional CO$_2$ emission is abated in all systems by replacing 2 PV panels with STCs, or even 3 in the case of system 5Gb. These STCs provide greater emission savings than the PV panels they replace by increasing the heat pump's COP due to higher borefield temperatures and by reducing the operation of the DHW heat pump.

Figure 6.9 shows 2D projections of the CO$_2$ graph slices. Additional emission savings relative to the full PV configuration are achieved by incorporating STCs, due to COP improvements and reduced DHW heat pump usage, up until the gray band.
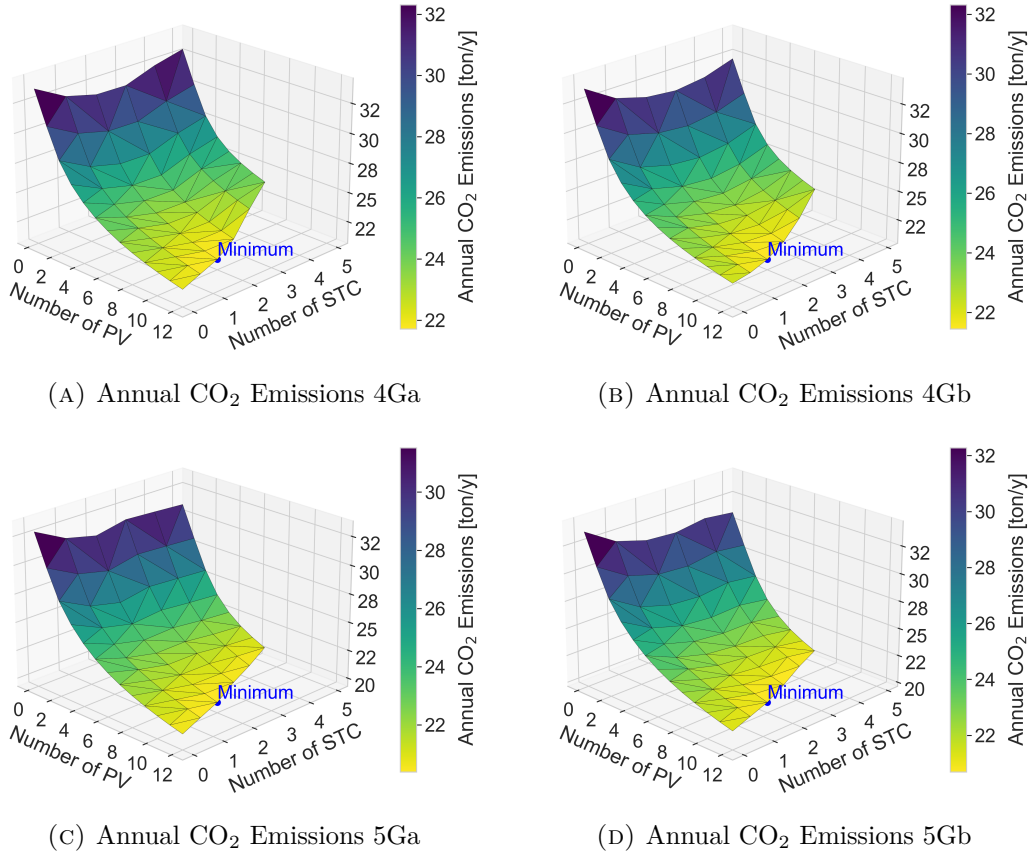
(A) Annual CO$_2$ Emissions 4Ga

(B) Annual CO$_2$ Emissions 4Gb

(C) Annual CO$_2$ Emissions 5Ga

(D) Annual CO$_2$ Emissions 5Gb

FIGURE 6.8: Annual CO$_2$ Emissions for different PV/STC configurations for all four systems

Beyond this point, adding more STCs results in increased electricity consumption for active cooling, which negates the additional CO$_2$ emission savings. Note that the b-systems have a greater capacity for borefield regeneration before active cooling emissions become dominant, as they have a larger borefield heat demand. When a significant number of collectors are added, Figures 6.9c and 6.9d show a decrease in annual emissions. This occurs because the borefield temperature becomes so elevated from regeneration that the increased COP emission savings start to outweigh the effects of active cooling. However, this potential optimum with a lot of STC is considered irrelevant because it comes with a very high TCO.

6.3   Total Cost of Ownership and CO$_2$ Emissions

Both performance indicators, the TCO, and the annual CO$_2$ emissions are combined in Figure 6.10. The figure illustrates both indicators for all systems, comparing the base case configuration with the configurations where the roof is fully covered with 12 panels. When both performance indicators improve by moving from one

(A) Annual CO$_2$ Emissions 4Ga

(B) Annual CO$_2$ Emissions 4Gb

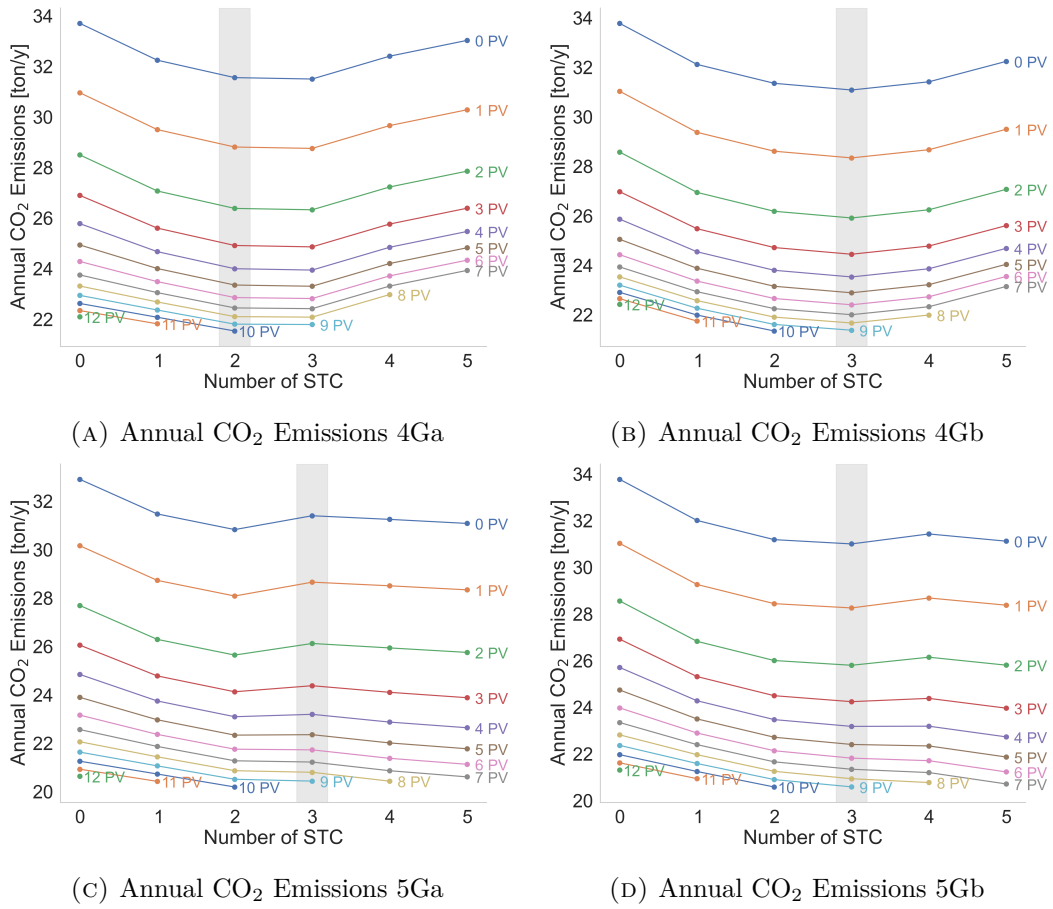(C) Annual CO$_2$ Emissions 5Ga

(D) Annual CO$_2$ Emissions 5Gb

FIGURE 6.9: 2D projection of Annual CO$_2$ Emissions graphs for different PV/STC configurations in all four systems (the number of STCs after which active cooling dominates is indicated in gray)

configuration to another, a Pareto improvement is achieved. This results in the more optimal points being positioned toward the lower-left corner of the plot.

In all four systems, a Pareto improvement is achieved when transitioning from the base case to the full PV configuration. For systems 4Gb and 5Gb, an additional Pareto improvement is realized by replacing a few PV panels with STCs, making these configurations the dominant choice for these systems. Comparing the Pareto-efficient solutions of the 4G and 5G systems, it is evident that the 4G systems are more cost-effective, while the 5G systems are more environmentally friendly. However, the cost increase associated with switching from a 4G to a 5G system is relatively high in relation to the emission reduction achieved. For example, comparing systems 4Gb and 5Ga in the 10PV/2STC configuration, the cost of abating CO$_2$ emissions over the project lifetime by switching from 4Gb to 5Ga is €9800 per ton CO$_2$. This cost is significantly higher compared to the average price of emission permits, which was around €75 per ton CO$_2$ in the European emission trading system over the past year
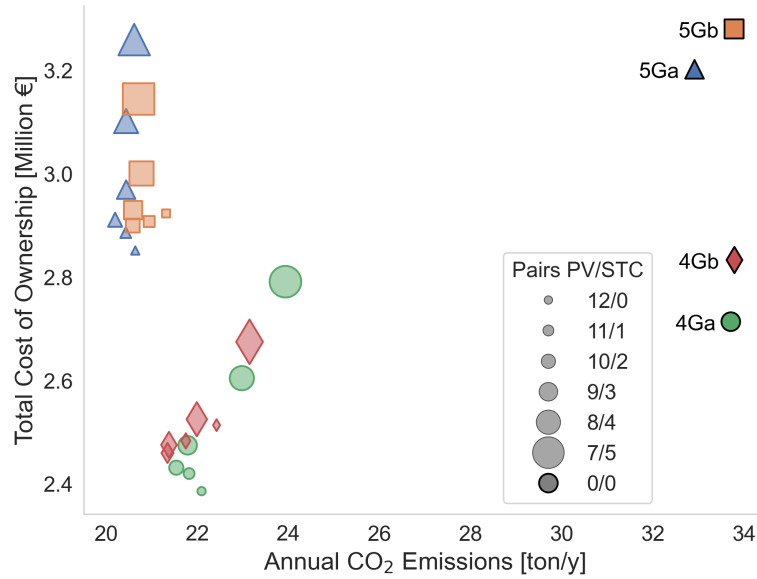
FIGURE 6.10: Total Cost of Ownership and Annual CO_2 Emissions for all four systems with full roof coverage configurations, and the 0PV/0STC configuration.

[55]. Therefore, the 5G systems are not considered to be overall effective solutions.

6.4 Sensitivity Analysis

This section conducts a one-at-a-time sensitivity analysis to assess how variations in individual parameters affect the economic and ecological trade-off between PV panels and STCs. The parameters investigated include the costs of PV panels, STCs, borefields, and electricity tariffs for feed-in and offtake. Additionally, the analysis examines the impact of increased space heating and cooling demand. The energy flow analysis is repeated with costs and demand profiles scaled from a 50% decrease to a 50% increase relative to the original values or profiles. The performance of system configurations with full roof coverage under these adjusted parameters is compared to their reference values, indicated by the green dashed line.

6.4.1 Sensitivity of Cost Parameters

Figure 6.11 displays the total cost of ownership for the system 4Ga PV/STC configurations with variations in several component investment costs. Variations in the PV panel investment cost do not significantly alter the optimal configuration, which remains full PV. A decrease in PV costs leads to a slightly higher total cost penalty when STCs are included, thereby favoring configurations with more PV panels. However, this effect is relatively minor. On the other hand, a 50% reduction in STC costs shifts the optimal configuration from full PV to one with 2 STCs, as illustrated in Figure 6.11b. This is a relevant sensitivity since significant cost reduction of STC

57

is expected as solar thermal energy will become more popular in the coming years, especially if considering the massive drop in PV cell cost due to R&D stimulating policies and economy of scale, when PV gained popularity [56, 57]. Figure 6.11c shows that variations in borefield cost have a minimal impact on the total cost of the system, without altering the optimal configuration of full PV. Systems with 3 STCs cause a reduction in borefield size and will therefore perform slightly better if the borefield cost increases.

(A) Variation PV Cost

(B) Variation STC Cost

(C) Variation Borefield Cost
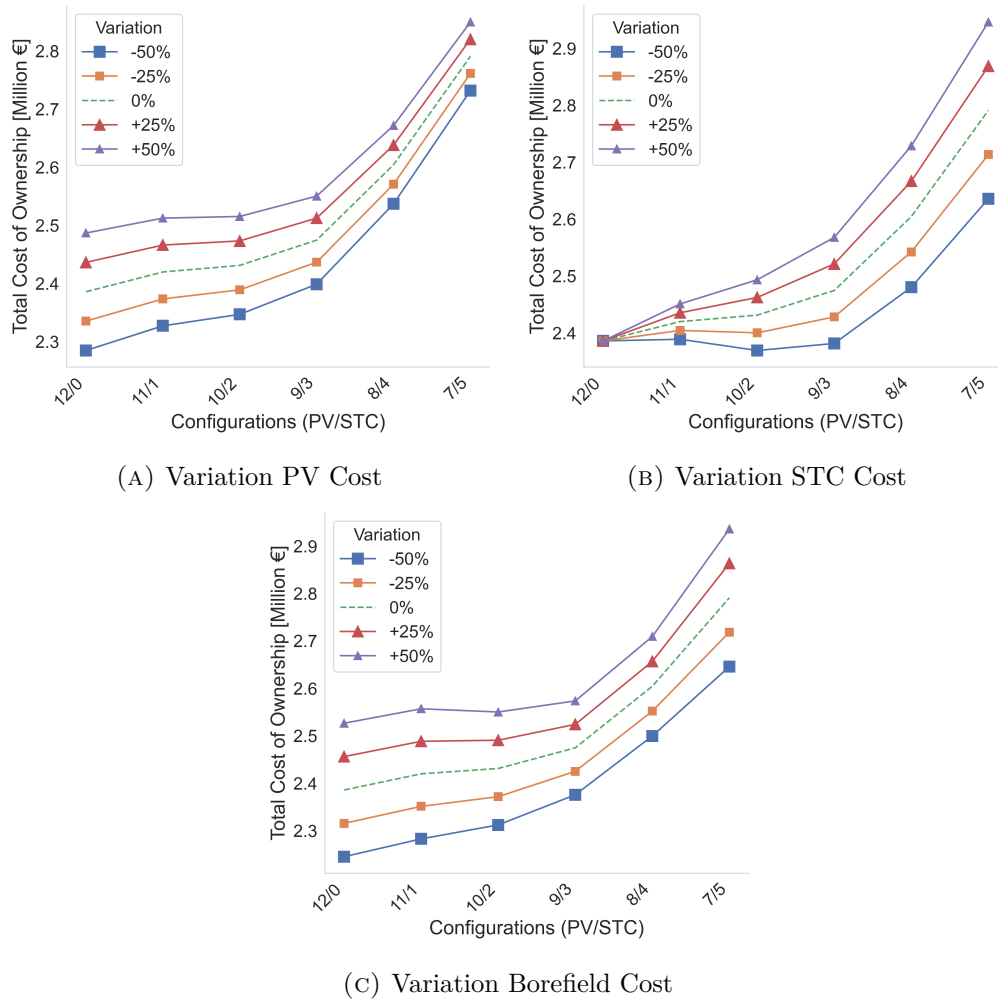
FIGURE 6.11: Effect of varying PV, STC and borefield investment costs on the Total Cost of Ownership for full roof coverage configurations in system 4Ga

A sensitivity analysis of the electricity tariffs affecting annual CO_2 emissions is shown in Figure 6.12. Electricity costs impact emissions by determining the feasibility of including a home battery in the system. A home battery allows for greater utilization of carbon-free PV electricity during periods of low solar irradiation, thus reducing grid demand. In the model, the battery is excluded from the system if it is deemed infeasible. The upper line in Figure 6.12a shows overlapping curves for

offtake tariffs where the battery is not included, demonstrating minimal CO_2 emissions with the 10PV/2STC configuration. As the electricity offtake tariff increases, the battery becomes feasible, causing the curves to shift to the lower line and resulting in significant emission savings. Under these conditions, the optimal configuration transitions to full PV as long as the battery remains feasible. A similar analysis applies to variations in the feed-in tariff, as shown in Figure 6.12b. The battery becomes feasible as the feed-in tariff decreases. This trend is particularly relevant for the future, considering the historical decrease in household electricity PV feed-in tariffs due to the increasing popularity of PV systems [58].

(A) Variation Electricity Offtake Tariff   (B) Variation Feed-in Offtake Tariff

FIGURE 6.12: Effect of varying the electricity offtake and feed-in tariff on the Annual CO_2 Emissions for full roof coverage configurations in system 4Ga

6.4.2 Sensitivity of Space Heating and Cooling Demand

Figure 6.13 illustrates the impact of scaled space heating and cooling demand profiles on the total cost of system 4Gb. An increase in space heating demand necessitates a larger borefield to meet this demand. Consequently, greater cost savings can be achieved through borefield regeneration, shifting the optimum configuration to one with more STCs, such as 9PV/3STC when the heating demand is increased by 50%. A similar analysis applies to decreased cooling demand. However, the effect is less pronounced, as no significant displacement in the optimal configuration is observed for the variations considered.

6.5 Reccomendations on PV and STC Utilization

This section combines relevant insights from this chapter to develop guidelines for the use of PV and STC systems in low-carbon residential heating districts equipped with a borefield storage unit. The selection process can be approached from both an economic perspective and an ecologically oriented perspective, as depicted in the

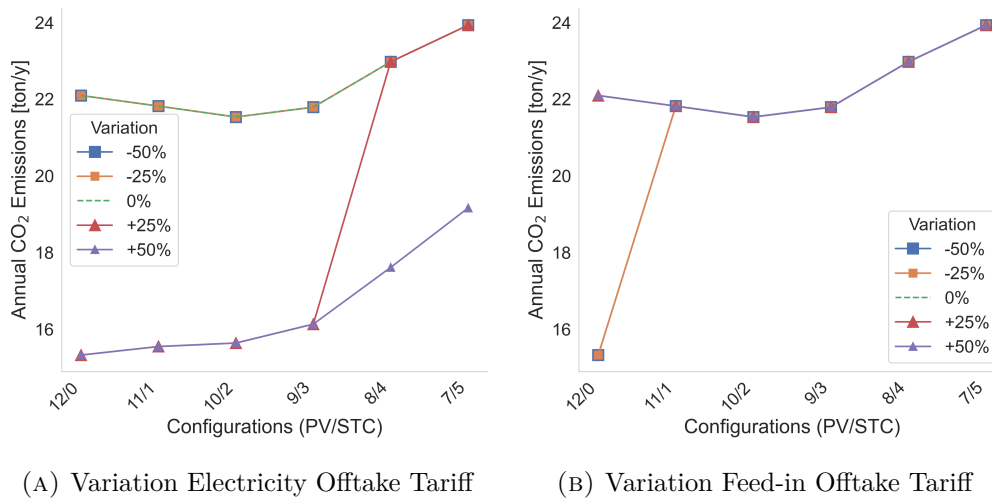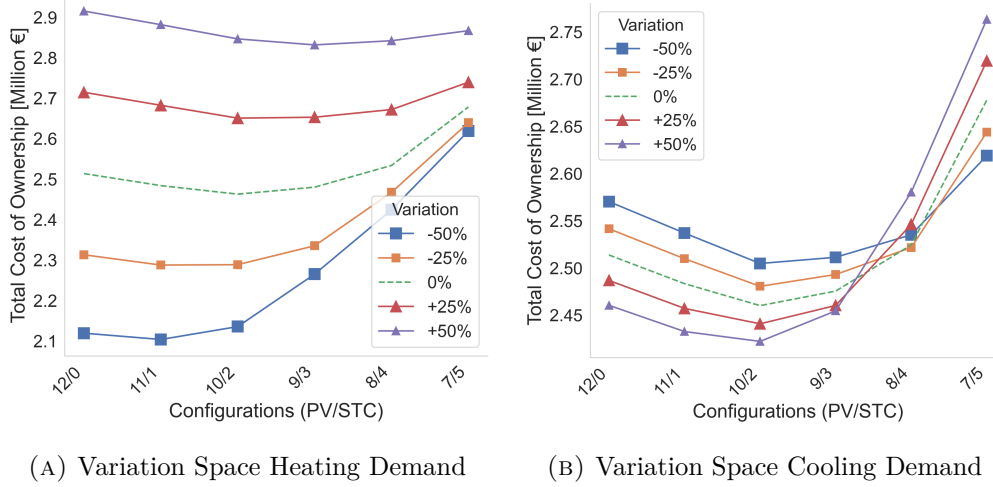(A) Variation Space Heating Demand   (B) Variation Space Cooling Demand

FIGURE 6.13: Effect of varying the space heating and cooling demand on the Total Cost of Ownership for full roof coverage configurations in system 4Gb

decision trees in Figure 6.14. In some cases, the optimal configuration from both perspectives may coincide, resulting in a Pareto-efficient solution.

- **Economic Perspective:** The decision-maker should evaluate the borefield size required to meet the heating and cooling demands. When borefield costs are high, especially in scenarios with large heating demand and relatively small cooling demand, a configuration that primarily uses PV panels with a limited number of STCs is preferred. The inclusion of STCs is limited by the maximum allowable borefield temperature, as excessive thermal regeneration causes a larger borefield and increases the electricity used for active cooling. If the cost savings from STCs do not justify their inclusion, the system should rely solely on PV panels.

- **Ecologic Perspective:** A decision-maker focused on minimizing operational CO_2 emissions would favor a configuration consisting entirely of PV panels if the system includes battery storage for PV-generated electricity. Without battery storage, a configuration with a combination of PV panels and a limited number of STCs will yield the lowest CO_2 emissions. The number of STCs is constrained by the potential increase in electricity demand for active cooling due to excessive regeneration.

Finally, some general recommendations can be made regardless of the specific perspective. As highlighted in Section 6.3, implementing PV and STC systems in a 4th-generation district heating system is generally recommended. The model indicates that the significant additional costs of a 5G system compared to a 4G, outweigh the benefits of reduced CO_2 emissions. Furthermore, it is important to
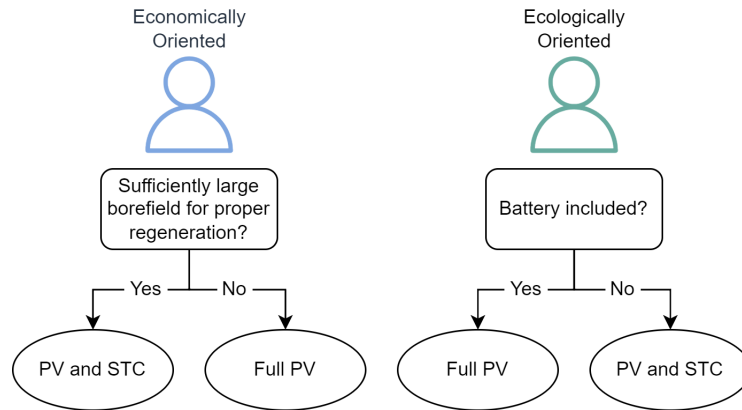
FIGURE 6.14: Decision trees from an economically and an ecologically oriented perspective

note that the use of both STC heat and PV electricity for the same goal, for instance, DHW generation, can negatively impact the cost savings of the system. Therefore, it is essential to consider a careful and thoughtful power allocation of the PV and STC generated energy.

Chapter 7

Conclusion and Recomendations

7.1 Conclusion

This thesis evaluates the performance of rooftop photovoltaic (PV) panels and solar thermal collectors (STCs) in collective residential energy systems from both economic and ecological perspectives. Virtual low-carbon residential energy systems incorporating PV and STC technologies are designed and assessed. These systems supply space heating, cooling, domestic hot water, and electricity to a district consisting of 50 low-energy dwellings, each with a floor area of 150 m^2.

Four low-carbon energy systems are designed based on literature and logical reasoning. These systems are optimized to integrate rooftop PV and STCs effectively, making the trade-off between them not trivial. Each system features a residential PV-home battery installation and a collective seasonal borehole thermal energy storage. The borefield storage is designed to store excess heat generated by STCs in summer for use in winter. For each system, an energy-flow model with hourly resolution is developed to calculate the Total Cost of Ownership (TCO) and operational CO_2 emissions. These metrics are used to assess the economic and ecological performance of the systems. The model uses data and synthetic load profiles corresponding to a Belgian environment. These load profiles represent the energy demand of a single dwelling, which is aggregated to form a district profile using a diversification factor. finally, the model evaluates the TCO and CO_2 emissions for various configurations of PV and STC installations to determine the trade-offs between them.

Based on the results, guidelines for the use of PV panels and STCs in collective residential energy systems can be established. Equipping the systems with only PV panels is a strong option from both economic and ecological perspectives. However, replacing some PV panels with STCs can yield additional cost savings in systems with a sufficiently large borefield, where STC thermal regeneration significantly reduces the borefield cost. Additionally, including some STCs can lower operational CO_2 emissions in systems that do not have a battery installed. The sensitivity analysis reveals that a decrease in STC costs, an increase in borefield costs, or a rise in heat

demand encourages the inclusion of more STCs in the cost-optimal configuration. On the other hand, an increase in the grid electricity offtake tariff or a decrease in the feed-in tariff shifts the ecological optimal configuration toward full PV. These trends are particularly relevant as the decreasing cost of STCs and reductions in feed-in tariffs are expected to be significant future developments.

7.2   Recomendations for Further Research

A first recommendation is to incorporate hybrid photovoltaic/thermal (PVT) panels into the trade-off analysis. PVT panels simultaneously generate electricity and heat, combining the benefits of PV and STC systems into a single technology. The PV cells in PVT panels are cooled by the heat generation process, which enhances their efficiency and extends their lifespan compared to conventional PV panels. Additionally, PVT panels require less space than separate PV and STC installations, making them particularly advantageous in urban areas where space is limited [30].

A second recommendation is to explore the impact of more optimized PV-generated electricity allocation. Electricity's versatility allows for enhanced performance through better control of electricity flow among various system components. For example, using excess PV electricity to regenerate borefield storage with a heat pump could mitigate the drawbacks of PV systems in high heat demand scenarios, where STC integration might otherwise be favored [59].

Finally, conducting a detailed simulation of the systems using tools such as *Modelica* is recommended. Integrating a thermocline in the domestic hot water tank model can improve STC efficiency and overall performance, potentially shifting the trade-off. A comprehensive system model that includes components like pumps, heat exchangers, and advanced control strategies could provide more precise and actionable guidelines for optimizing these energy systems.

Appendices

Appendix A

Component Cost Data

Component	Investment Cost [€]	X
Solar Thermal Collector	803	-
Domestic Hot Water tank	1834	-
Air-Water DHW HP	3142	-
Booster DHW HP	4414	-
Residential HP	$429 \cdot X + 8307$	Heating power [kW]
Photovoltaic Panel	183	-
Hybrid Converter	$81 \cdot X + 416$	Electric power [kW]
Home Battery	$500 \cdot X$	Capacity [kWh]
District Heating Network High T	$400 \cdot X$	HT network lenght [m]
District Heating Network Low T	$250 \cdot X$	LT network lenght [m]
Buffer Tank	$750 \cdot X + 404 \cdot X^{0.532}$	Volume [m^3]
Central HP	$189 \cdot X + 11440$	Heating power [kW]
Borefield	$35 \cdot X$	Borefield length [m]
Component	Annual Maintenance	# Investments
Solar Thermal Collector	1%	2
Domestic Hot Water tank	2%	2
Air-Water DHW HP	2%	2
Booster DHW HP	2%	2
Residential HP	2%	2
Photovoltaic Panel	1%	2
Hybrid Converter	0.5%	3
Home Battery	0.5%	3
District Heating Network High T	0.5%	1
District Heating Network Low T	0.5%	1
Buffer Tank	0.5%	1
Central HP	2%	2
Borefield	0.5%	1

TABLE A.1: Overview of component cost data: investment cost curve, annual maintenance cost as a percentage of the investment cost, and number of investments in 40 years [9, 8, 19, 20, 21, 22, 10, 23, 7, 24, 14]

Bibliography

[1] D. N. Energy, "Introduction to hybrid solar system." `https://www.dsneg.com/info/introduction-to-hybrid-solar-system-36455075.html`, 2019. Accessed: 2024.

[2] A. Greco, E. Gundabattini, D. S. Gnanaraj, and C. Masselli, "A comparative study on the performances of flat plate and evacuated tube collectors deployable in domestic solar water heating systems in different climate areas," *Climate*, vol. 8, no. 6, 2020.

[3] C. O. Suong and A. Asanakham, "Evaluation of a single stage heat pump performance by figure of merit (fom)," *Energy Reports*, vol. 6, pp. 2735–2742, 11 2020.

[4] "Borehole Thermal Energy Storage: DLSC — dlsc.ca." `https://www.dlsc.ca/borehole.htm`. [Accessed 28-05-2024].

[5] M. Y. Haller, C. A. Cruickshank, W. Streicher, S. J. Harrison, E. Andersen, and S. Furbo, "Methods to determine stratification efficiency of thermal energy storage processes – review and theoretical comparison," *Solar Energy*, vol. 83, no. 10, pp. 1847–1860, 2009.

[6] P. Wallentén, *Steady-state heat loss from insulated pipes.* Licentiate thesis, Division of Building Physics, 1991.

[7] M. Coninx, J. De Nies, L. Hermans, W. Peere, W. Boydens, and L. Helsen, "Cost-efficient cooling of buildings by means of geothermal borefields with active and passive cooling," *Applied Energy*, vol. 355, p. 122261, 2024.

[8] D. E. N.V., "Verwarmingscatalogus - residentiële oplossingen." `https://docplayer.nl/188196957-Verwarmingscatalogus-residentieleoplossingen.html`, 2020. Accessed: 2024.

[9] Buderus, *Prijslijst 1 – Residentiële installaties*, 2021.

[10] L. Hermans, R. Haesen, A. Uytterhoeven, W. Peere, W. Boydens, and L. Helsen, "Pre-design of collective residential solar districts with seasonal thermal energy

storage: Importance of level of detail," *Applied Thermal Engineering*, vol. 226, p. 120203, 2023.

[11] D. E. N.V., "User, installations and maintenance manual - domestic hot water heat pump monobloc type." `https://www.daikin.dk/content/dam/document-library/installation-manuals/heat/domestic-hot-water-heat-pump/EKHHE-CV3,EKHHE-PCV3_Installation%20and%20operation%20manual_English.pdf`. Accessed: 2024, p. 12.

[12] N. E. B.V., "Nibe prijscatalogus belgië." `https://nibe.eu/assets/documents/26317/Handleiding%20MT-MB21-019%20booster%20warmtepomp%2005-2019%20NL.pdf`. Accessed: 2024, p. 23.

[13] Viessmann, "Technical guide - brine/water and water/water heat pump 1-stage and 2-stage, 1.7 to 117.8 kw." `https://viessmanndirect.co.uk/files//499b1238-03e0-4b0c-b7d5-adda016de3ff/Technical%20Guide.pdf`. Accessed: 2024, p. 11.

[14] R. Haesen and L. Hermans, "Design and assessment of low-carbon residential district concepts with (collective) seasonal thermal energy storage," master's thesis, KU Leuven, 2021.

[15] Logstor, *Product Catalogue - District Energy*, December 2020.

[16] Trinasolar, "vertex s backsheet monocrystalline module - product:tsm-de09r.05." `https://a93d26b8-fdab-4769-998a-8067230d1667.usrfiles.com/ugd/a93d26_d1e3b21e04a7441da2c09208cb57a54b.pdf`, 2022. Accessed: 2024.

[17] Huawei, "Smart energy controller." `https://solar.huawei.com/en/download?p=%2F-%2Fmedia%2FSolar%2Fattachment%2Fpdf%2Fau%2Fdatasheet%2FSUN2000-5_6KTL-M0.pdf`, 2020. Accessed: 2024.

[18] D. Parra and M. K. Patel, "The nature of combining energy storage applications for residential battery technology," *Applied Energy*, vol. 239, pp. 1343–1355, 2019.

[19] Avenir, "Pompe à chaleur géothermie." `https://www.avenir-renovations.fr/boutique/chauffage-et-plomberie/chauffage/pac-pompe-a-chaleur/pompe-a-chaleur-geothermie/vitocal-200-g-pompes-a-chaleur-v1.html`. Accessed: 2024.

[20] Solar@Home, "Trina solar vertex s (r) 415w triple-cut full black (w15y)." `https://www.solarathome.be/product-page/trina-solar-vertex-s-r-415w-triple-cut-full-black-w15y`. Accessed: 2024.

[21] S. Shop, "hybrid inverters." `https://wsolar.shop/en/hybrid-inverters?_gl=1*19f2yr8*_up*MQ..&gclid=`

`Cj0KCQjw6PGxBhCVARIsAIumnWbUn09arxiVBN9r2ZnZuCa1c55BIW_`
`7d1AILFZW-drSHiAun5hnjGUaAucJEALw_wcB`. Accessed: 2024.

[22] S. Shop, "battery packs." `https://wsolar.shop/`
`en/battery-packs?_gl=1*l7myq2*_up*MQ..&gclid=`
`Cj0KCQjw6PGxBhCVARIsAIumnWbUn09arxiVBN9r2ZnZuCa1c55BIW_`
`7d1AILFZW-drSHiAun5hnjGUaAucJEALw_wcB`. Accessed: 2024.

[23] F. Mauthner and S. Herkel, "Iea shc task52 - deliverable c1: Classification and benchmarking of solar thermal systems in urban environments," 05 2017.

[24] Huawei, "Smart string energy storage system." `https://solar.huawei.com/`
`en/professionals/all-products/LUNA2000-7-14-21-S1`. Accessed: 2024.

[25] European Commission, "New rules for greener and smarter buildings will increase quality of life for all europeans." `https://ec.europa.eu/info/news/`
`new-rules-greener-and-smarter-buildings-will-increase-quality-life-all-europeans-2`
`en`, 2019. Accessed: 2024-08-10.

[26] European Environment Agency, "Greenhouse gas emissions from energy use in buildings in europe." `https://www.eea.europa.eu/en/analysis/`
`indicators/greenhouse-gas-emissions-from-energy`, 2023. Accessed: 2024-08-10.

[27] M. Zukowski, M. Kosior-Kazberuk, and T. Blaszczynski, "Energy and environmental performance of solar thermal collectors and pv panel system in renovated historical building," *Energies*, vol. 14, no. 21, p. 7158, 2021.

[28] F. Huide, Z. Xuxin, M. Lei, Z. Tao, W. Qixing, and S. Hongyuan, "A comparative study on three types of solar utilization technologies for buildings: Photovoltaic, solar thermal and hybrid photovoltaic/thermal systems," *Energy Conversion and Management*, vol. 140, pp. 1–13, 2017.

[29] M. Jiang, C. Rindt, and D. Smeulders, "Optimal planning of future district heating systems—a review. energies. 2022; 15: 7160," 2022. Accessed: 2024.

[30] A. H. A. Al-Waeli, H. A. Kazem, M. T. Chaichan, and K. Sopian, *Photovoltaic/Thermal (PV/T) Systems: Principles, Design, and Applications*. Springer International Publishing AG, 1st ed. 2019. ed., 2019.

[31] K. Ndwali, J. G. Njiri, and E. M. Wanjiru, "Multi-objective optimal sizing of grid connected photovoltaic batteryless system minimizing the total life cycle cost and the grid energy," *Renewable Energy*, vol. 148, pp. 1256–1265, 4 2020.

[32] F. Fiedler and J. C. Matas, "Techno-economic analysis of grid-connected pv battery solutions for holiday homes in sweden," *Energies*, vol. 15, 4 2022.

[33] Enertrik, "User manual - hybrid 5.5kw pv inverter." `https:`
`//enertik.com/wp-content/uploads/sites/2/documentos/manuales/`
`manual-inversor-solar-hibrido-hgi-55k-48.pdf`. Accessed: 2024.

[34] V. B. BV, "Technical guide - solar thermal systems." https://www.vitosol.nl/vitosol/3000/pdf/handboek/handboek_GB.pdf, 2009. Accessed: 2024.

[35] H. Charlick and I. Summerfield, "Investigation of the interaction between hot water cylinders, buffer tanks and heat pumps," *Kiwa GASTEC at CRE, Department of Energy and Climate Change, Cheltenham, UK*, 2013.

[36] M. Dannemand, B. Perers, and S. Furbo, "Performance of a demonstration solar pvt assisted heat pump system with cold buffer storage and domestic hot water storage tanks," *Energy and buildings*, vol. 188-189, pp. 46–57, 2019.

[37] H. Hemmatabady, J. Formhals, B. Welsch, D. O. Schulte, and I. Sass, "Optimized layouts of borehole thermal energy storage systems in 4th generation grids," *Energies*, vol. 13, no. 17, 2020.

[38] J. Schlund, N. Pflugradt, D. Steber, U. Muntwyler, and R. German, "Benefits of virtual community energy storages compared to individual batteries based on behaviour based synthetic load profiles," in *2018 IEEE PES Innovative Smart Grid Technologies Conference Europe (ISGT-Europe)*, pp. 1–6, IEEE, 2018.

[39] B. J. Kalkbrenner, "Residential vs. community battery storage systems–consumer preferences in germany," *Energy Policy*, vol. 129, pp. 1355–1363, 2019.

[40] H. Hemmatabady, J. Formhals, B. Welsch, D. O. Schulte, and I. Sass, "Optimized layouts of borehole thermal energy storage systems in 4th generation grids," *Energies*, vol. 13, no. 17, p. 4405, 2020.

[41] H. Hens, *Toegepaste bouwfysica en installaties in gebouwen: koeling, luchtbehandeling.* Leuven: Acco, 3rd, revised edition ed., 2008.

[42] GitHub, "Github copilot." https://github.com/features/copilot, 2024. Accessed: 2024-08-10.

[43] OpenAI, "Gpt-4." https://openai.com/research/gpt-4, 2023. Accessed: 2023-08-10.

[44] I. Pakere and D. Blumberga, "Solar power or solar heat: What will upraise the efficiency of district heating? multi-criteria analyses approach," *Energy (Oxford)*, vol. 198, pp. 117291–, 2020.

[45] D. Clark, *What Colour is your Building?: Measuring and reducing the energy and carbon footprint of buildings.* RIBA Publishing, 2019.

[46] Engie, "Wat is het injectietarief?." https://www.engie.be/nl/injectie-zonnepanelen/. Accessed: 2024.

[47] Sibelga, "What is the average electricity and gas consumption in the brussels region?." https://www.energuide.be/en/questions-answers/what-is-the-average-electricity-and-gas-consumption-in-the-brussels-region/273/, 2024.

[48] nPro, "Load profiles for residential buildings." https://www.npro.energy/main/en/load-profiles/residential. Accessed 30-06-2024.

[49] Daiking, "Heat recovery hot water system." https://www.daikin.com.sg/product-series/vrv-hw/. Accessed: 2024-08-10.

[50] M. Garciá-Rincón, J. Flores-Prieto, and O. Montoya-Márquez, "Thermal performance of a low and medium temperature flat plate solar collector when controlling the output-input temperature difference and the tilt angle," *Journal of Solar Energy Engineering*, vol. 144, no. 2, p. 021008, 2022.

[51] nPro, "Diversity factors in district heating networks." https://www.npro.energy/main/en/district-heating-cooling/diversity-factor. Accessed 30-06-2024.

[52] Viessmann, "Technical guide - vitocal 300-g pro." https://cdn0.scrvt.com/2828ebc457efab95be01dd36047e3b52/04394dd499bd19e8/8d9c1ff0f4ec/Vitocal-300-G-Pro-Technical-Guide.PDF. Accessed: 2024, p. 15.

[53] W. Peere, D. Picard, I. Cupeiro Figueroa, W. Boydens, and L. Helsen, "Validated combined first and last year borefield sizing methodology.," in *Building Simulation 2021*, vol. 17, pp. 49–55, IBPSA, 2021.

[54] F. L. P. V. D. Bossche and G. V. Lysebetten, *Ondiepe Geothermie - Ontwerp en Uitvoering van Bodemenergiesystemen met U-vormige Bodemwarmtewisselaars*, 2016.

[55] T. economics, "Eu carbon permits." https://tradingeconomics.com/commodity/carbon. Accessed: 2024.

[56] B. Köhler, M. Stobbe, C. Moser, and F. Garzia, "Guideline ii: nzeb technologies: Report on cost reduction potentials for technical nzeb solution sets," *Fraunhofer Institute for Solar Energy Systems: Freiburg, Germany*, 2018.

[57] G. Kavlak, J. McNerney, and J. E. Trancik, "Evaluating the causes of cost reduction in photovoltaic modules," *Energy Policy*, vol. 123, pp. 700–710, 2018.

[58] H. Schwarz, H. Schermeyer, V. Bertsch, and W. Fichtner, "Self-consumption through power-to-heat and storage for enhanced pv integration in decentralised energy systems," *Solar Energy*, vol. 163, pp. 150–161, 2018.

[59] M. C. Fotopoulou, P. Drosatos, S. Petridis, D. Rakopoulos, F. Stergiopoulos, and N. Nikolopoulos, "Model predictive control for the energy management in a district of buildings equipped with building integrated photovoltaic systems and batteries," *Energies*, vol. 14, no. 12, p. 3369, 2021.